The Aqua-Planet Experiment (APE): Response to changed meridional SST profile

David L. Williamson[1], Michael Blackburn[2], Kensuke Nakajima[3], Wataru Ohfuchi[4], Yoshiyuki O. Takahashi[5], Yoshi-Yuki Hayashi[5], Hisashi Nakamura[6], Masaki Ishiwatari[7], John L. McGregor[8], Hartmut Borth[9], Volkmar Wirth[10], Helmut Frank[11], Peter Bechtold[12], Nils P. Wedi[12], Hirofumi Tomita[13], Masaki Satoh[14], Ming Zhao[15], Isaac M. Held[15], Max J. Suarez[16], Myong-In Lee[17], Masahiro Watanabe[18], Masahide Kimoto[18], Yimin Liu[19], Zaizhi Wang[20], Andrea Molod[21], Kavirajan Rajendran[22], Akio Kitoh[23] and Rachel Stratton[24]

[1]National Center for Atmospheric Research, Boulder, CO, USA
[2]National Centre for Atmospheric Science, The University of Reading, Berkshire, UK
[3]Kyushu University, Kyushu, Japan
[4]Japan Agency for Marine-Earth Science and Technology, Japan
[5]Kobe University, Kobe, Japan
[6]The University of Tokyo, Tokyo, Japan
[7]Hokkaido University, Hokkaido, Japan
[8]CMAR, Aspendale, Australia
[9]Theoretical Meteorologie, University of Hamburg, Hamburg, Germany
[10]Institute for Atmospheric Physics, University of Mainz, Mainz, Germany
[11]Research and Development, Deutscher Wetterdienst, Offenbach, Germany
[12]European Centre for Medium Range Weather Forecasts, Reading, Berkshire, UK
[13]Advanced Institute for Computational Science, RIKEN, Japan
[14]Atmosphere and Ocean Research Institute, University of Tokyo, Kashiwa, Japan
[15]Geophysical Fluid Dynamics Laboratory, Princeton University, Princeton, NJ, USA
[16]GMAO, NASA Goddard Space Flight Center, Greenbelt, MD, USA
[17]Ulsan National Institute of Science and Technology, Korea
[18]Atmosphere and Ocean Research Institute, The University of Tokyo, Japan
[19]LASG, Institute of Atmospheric Physics, CAS, Beijing, China
[20]National Climate Center, China Meteorological Administration, China
[21]GMAO, NASA Goddard Space Flight Center, Greenbelt, MD, USA
[22]C-MMACS, National Aerospace Laboratories, Bangalore, India
[23]Meteorological Research Institute, Tsukuba, Japan
[24]Met Office, Exeter, Devon, UK

Journal of the Meteorological Society of Japan
Special Issue on the Aqua-Planet Experiment

Submitted 8 August 2011

Revised 9 March 2012

Final form 30 November 2012

Corresponding author's address: Michael Blackburn, National Centre for Atmospheric Science, Department of Meteorology, University of Reading, Earley Gate, PO Box 243, Reading, RG6 6BB, UK (e-mail: m.blackburn@reading.ac.uk)

Abstract

This paper explores the sensitivity of Atmospheric General Circulation Model (AGCM) simulations to changes in the meridional distribution of sea surface temperature (SST). The simulations are for an aqua-planet, a water covered Earth with no land, orography or sea-ice and with specified zonally symmetric SST. Simulations from 14 AGCMs developed for Numerical Weather Prediction and climate applications are compared. Four experiments are performed to study the sensitivity to the meridional SST profile. These profiles range from one in which the SST gradient continues to the equator to one which is flat approaching the equator, all with the same maximum SST at the equator. The zonal mean circulation of all models shows strong sensitivity to latitudinal distribution of SST. The Hadley circulation weakens and shifts poleward as the SST profile flattens in the tropics. One question of interest is the formation of a double versus a single ITCZ. There is a large variation between models of the strength of the ITCZ and where in the SST experiment sequence they transition from a single to double ITCZ. The SST profiles are defined such that as the equatorial SST gradient flattens, the maximum gradient increases and moves poleward. This leads to a weakening of the mid-latitude jet accompanied by a poleward shift of the jet core. Also considered are tropical wave activity and tropical precipitation frequency distributions. The details of each vary greatly between models, both with a given SST and in the response to the change in SST. One additional experiment is included to examine the sensitivity to an off-equatorial SST maximum. The upward branch of the Hadley circulation follows the SST maximum off the equator. The models that form a single precipitation maximum when the maximum SST is on the equator shift the precipitation maximum off equator and keep it centered over the SST maximum. Those that form a double with minimum on the equatorial maximum SST shift the double structure off the equator, keeping the minimum over the maximum SST. In both situations only modest changes appear in the shifted profile of zonal average precipitation. When the upward branch of the Hadley circulation moves into the hemisphere with SST maximum, the zonal average zonal, meridional and vertical winds all indicate that the Hadley cell in the other hemisphere dominates.

1 Introduction

The Aqua-Planet Experiment (APE) consists of a series of Atmospheric General Circulation Model (AGCM) simulations on a variety of water covered planets which otherwise have Earth-like physical characteristics. The experiment involves a comparison of a number of AGCMs which are used for or are being developed for climate and numerical weather prediction applications. The AGCMs are complete as developed for Earth applications but are applied to an idealized water covered planet with no land, orography or sea-ice. The Sea Surface Temperatures (SST) are specified to have simple distributions and are fixed in time. A modest number of SST fields, to be described below, are specified in order to study the response of aqua-planet simulations to changes in the SST fields. In this paper we consider the response to changes in the meridional SST profile and the response to shifting the maximum SST off the equator.

APE was conceived by Neale and Hoskins (2000a) as one component of a modelling hierarchy of increasing complexity, both of the models themselves and of the experimental configurations to which they are applied. The hierarchy has two distinct roles: an evaluation role in the development and testing of complex atmospheric models, and a conceptual role in linking complex models with theory and observation. This context of APE is discussed in more detail by Blackburn and Hoskins (2013), so only a summary is given here.

In the conceptual context, theory and more idealised models provide constraints on the character of the global circulation expected in APE. The zonally averaged SST distributions in APE are broadly similar to Earth, so the equator-to-pole temperature difference is expected to give rise to a jet stream and storm track in mid-latitudes. Theory suggests that the location and strength of the storm track will closely follow low-level baroclinicity associated with the mid-latitude SST gradient. Recent idealised modelling studies (Lu et al., 2010; Butler et al., 2011) have highlighted the importance of changes in static stability in influencing the latitude of maximum baroclinic instability, suggesting that increased sub-tropical static stability may be one mechanism that causes the storm tracks to migrate polewards in simulations of 21st century climate warming (Yin, 2005; Lorenz and DeWeaver, 2007).

In the tropics, the analytic model of Held and Hou (1980) predicts that a Hadley circulation with equatorial ascent must exist when the latitudinal profile of temperature in equilibrium with the underlying SSTs is steeper than quartic, in order to maintain a themal wind balance consistent with angular momentum conservation. The tropical SST profiles in APE were designed to include this limiting case: they vary from a profile denoted PEAKED in which the mid-latitude SST gradient extends to the equator, through a CONTROL which is quadratic and QOBS which is closer to the observed profile in the Pacific, to a quartic profile denoted FLAT. The tropical circulation is therefore expected to consist of a Hadley circulation with equatorial ascent for the steeper SST profiles, but this should break down in the limiting FLAT case to give a state closer to radiative-convective equilibrium at each latitude.

Held and Hou (1980) considered only forcing and SSTs symmetric about the equator in their analytic and idealised numerical model study. Later, Lindzen and Hou (1988) found that moving the SST maximum only a few degrees off the equator resulted in a marked asymmetry of the Hadley cells, with rising on the summer side of the equator and a much strengthened cell crossing the equator into the winter hemisphere. In order to test this asymmetry in AGCM simulations, Neale and Hoskins (2000a) proposed a fifth zonally symmetric forcing case in which the SST maximum is moved 5° off the equator, CONTROL_5N.

Previous modelling studies using aqua-planet configurations have confirmed that the tropical circulation and the location of the Inter-Tropical Convergence Zone (ITCZ) produced by AGCMs do depend on SST. The most systematic study, by Hess et al. (1993), used a number of widely varying tropical SST profiles and two different convective parameterizations in a single model. Hess et al. and other studies found that the tropical circulation and ITCZ location also differs between models, with some models producing a double-ITCZ straddling the equator even when SST is peaked on the equator. Such a double-ITCZ was found in the first modern aqua-planet simulation, by Hayashi and Sumi (1986). An unrealistic double-ITCZ is also found in many simulations using coupled atmosphere-ocean GCMs (e.g. Lin, 2007). As discussed in Blackburn and Hoskins (2013), the origin of this phenomenon and its relationship to uncoupled simulations with prescribed SSTs are not well understood.

A number of these studies, in particular that of Hess et al., provided motivation for Neale and Hoskins (2000a) to propose a benchmark test suite of AGCM aqua-planet experiments. In this evaluation context of the modelling hierarchy, APE is a bridge between experiments with models of reduced complexity that are used in the development of individual model components, and realistic simulations of Earth's climate using complete AGCMs, coordinated through the Atmospheric Model Intercomparison Project (AMIP, described in its original form by Gates, 1992). APE therefore provides a test-bed for the interaction of dynamics and physical parameterizations in AGCMs which is simpler than Earth yet contains the complete sub-gridscale parameterization package developed for Earth applications. For this reason, APE is sponsored by the Working Group on Numerical Experimentation (WGNE) which is jointly sponsored by the World Meteorological Organization (WMO) Commission on Atmospheric Science (CAS) and World Climate Research Program (WCRP). The goals of APE are to expose inter-model differences, to stimulate research to understand their causes and to provide a benchmark of the behaviors of the current generation of models.

This paper considers the simulated responses to varying the latitudinal profile of SST, using experiments based on the five zonally symmetric SST distributions defined by Neale and Hoskins. A companion paper, Blackburn et al. (2013), discusses the CONTROL SST experiment in more detail.

2 Experimental Design and Participating Models

The latitudinal structures of the five zonally symmetric SST fields are shown in Fig. 1. The simple formulae defining these distributions are not repeated here but were originally given in Neale and Hoskins (2000a) and are repeated in Blackburn and Hoskins (2013) and Williamson et al. (2012). The four latitudinally symmetric distributions, labeled PEAKED, CONTROL, QOBS and FLAT, have a maximum SST of 27C at the equator and differ in their meridional gradients approaching the equator. All experiments specify a SST of 0C poleward of 60° latitude, with no sea ice. The PEAKED experiment has a strong SST gradient continuing to the equator while the FLAT experiment has its maximum gradient poleward of 20° latitude and is quartic in latitude, giving a broad equatorial SST maximum and flatter profile approaching the equator. The CONTROL SST is quadratic in latitude and QOBS is the average of CONTROL and FLAT. Based on their experience with the Met Office model (HadAM3, Pope et al., 2000) applied to these SST fields, Neale and Hoskins (2000a) designated the CONTROL as the standard experiment. However, QOBS is closest to the observed zonal mean boreal winter SST in the Pacific. The fifth SST, denoted CONTROL_5N, distorts the CONTROL SST by shifting the maximum to 5°N while holding the transition to 0C fixed at ±60° latitude. As discussed in the introduction, the four hemispherically symmetric SSTs are intended to study the issue of the intensity of the ITCZ and the formation of a single ITCZ on the equator versus a double ITCZ spanning the equator. The hemispherically asymmetric SST is intended to examine the response of the ITCZ when the maximum SST is not on the equator.

The APE design included certain model specifications in order to obtain uniformity across the models. Complete details are available on the APE web site (http://climate.ncas.ac.uk/ape/) and in an atlas of model simulation statistics (Williamson et al., 2012), hereafter referred to simply as the ATLAS. Many aspects of the design are also briefly summarized in Blackburn et al. (2013) and Blackburn and Hoskins (2013). Values for basic geophysical constants and parameters are recommended. The insolation is perpetual equinoctial and symmetric about the equator, but includes the diurnal cycle. Values are specified for the solar constant and CO_2 concentration. Recommendations are given for other well mixed gasses as well as for the mass of the dry atmosphere. Ozone is specified as a zonally and meridionally symmetric latitude-height distribution determined from the annual mean climatology used in AMIP II (Wang et al., 1995; Liang and Wang, 1996).

The simulations are run for 3.5 years for each experiment. The analysis is made over the last

3 years, omitting the first 6 months as spin-up. A model-simulated state, from either a previous aqua-planet integration or an earth-like simulation, should be used for the initial conditions. In independent tests of the spin-up in several models, aqua-planet climate equilibrated in a matter of weeks from these types of initial condition, so a 6 month spin-up is considered adequate. Nevertheless, the modelling groups were instructed to check that equilibration was achieved during the discarded initial 6-month period. Daily time-series of global averages were requested for a number of variables, which allows a gross check that equilibrium was reached. A variety of data sets from the final three years of the simulations was requested for the APE data archive. This list is considerably longer than that suggested by Neale and Hoskins (2000a) and is given on the APE web site (http://climate.ncas.ac.uk/ape/) and summarized in the ATLAS.

Simulations from 16 models were contributed to the APE data base. These models are listed in Table 1. The table includes the commonly accepted model name, the group that contributed the data and the location of the group's home institution. The group symbol is used to identify the models in figures, tables and discussions. Not all models contributed simulations for all SST distributions. The last two columns of Table 1 indicate those that contributed PEAKED, CONTROL, QOBS and FLAT and those that contributed CONTROL and CONTROL_5N. Those are the models analyzed here. The models include established models that have been used in production applications such as numerical weather prediction and IPCC simulations, and some newer, more novel models that have been less well tested in real-world applications. Table 2 summarizes the dynamical cores, the methods used for water vapor transport and resolutions of the participating models. Table 3 lists major choices in the model parameterizations of convection and boundary layer turbulence. Brief descriptions of the models with references for their algorithms are available in the ATLAS.

The simulations from the CONTROL experiment are presented in a companion paper (Blackburn et al., 2013). Most of the figures included there and in the current paper are extracted from the ATLAS. Because of the number of experiments considered (five) and number of models involved (fourteen of the sixteen submitted) we can only provide a sampling of the properties of the aqua-planet simulations and an indication of the wide variety of model behaviors. Detailed analyses are left for individual studies of specific aspects. We summarize the collective APE model behavior for many statistics with a multi-model mean. The statistics are always calculated on each model's submitted data grid, then linearly interpolated to a 1° latitude-longitude grid to calculate the multi-model mean. A more complete description of the process is given in the ATLAS. The models are weighted equally for the mean even though with some statistics

there are model outliers. The sample size is large enough that the impact of outliers is generally small, although there are a few exceptions. One subtle aspect is that the models included in the multi-model mean for the CONTROL depend on which experiments it is being compared to. Thus in Blackburn et al. (2013), which considered only the CONTROL experiment, the multi-model mean includes all models in Table 1 except FRCGC which is an extremely high resolution model and was only run for 30 days. The multi-model mean for the PEAKED, CONTROL, QOBS, FLAT comparison here includes all models with an X in the next-to-last column in Table 1. The multi-model mean for the CONTROL_5N, CONTROL comparison later includes all models with an X in the last column in Table 1. Thus plots of the CONTROL for the multi-model mean will not be identical in the different comparisons. The multi-model mean should not be thought of as a best estimate of the aqua-planet climate. It is simply a convenient way to summarize the properties of the current set of AGCMs. In this set, no one model is a good match for the multi-model mean, and in general the individual models all differ from the multi-model mean.

To indicate variations among the APE models we present the inter-model standard deviation. The standard deviation of the statistics is also calculated after the statistics for each model are calculated on the submitted model grid and interpolated to the 1° grid. As with the multi-model mean, the models are weighted equally for the standard deviation even though with some statistics there are model outliers. These outliers do have a noticeable effect on some of the standard deviations. The corresponding plots for all individual models are available in the ATLAS but we do not provide specific figure numbers here. When discussing the multi-model mean and inter-model standard deviation, we often describe in words the source of the variability between models. This is our subjective evaluation of the plots from all the individual models contained in the ATLAS. These overviews are intended to emphasize the great variation between the models in most of the statistics examined.

As noted above and as can be seen in the ATLAS, there are 3 or 4 models that are relative outliers in many metrics. These do affect the multi-model mean climate to some extent, but probably have a larger effect on the inter-model standard deviations. Nevertheless we perform all analyses with the complete set of models. All contributed models were accepted into the APE data base with no overall quality criterion. In fact, applying a quality cut-off would be particularly difficult since the APE climate is unknown. Perhaps criteria could be based on the quality of Earth-like simulations but even then only egregious outliers could be safely discarded. APE outliers only become apparent in the comparative analyses, and there is a

remote possibility that they provide a more accurate indication of the APE climate. We provide plots of some statistics for individual models as well. Individual model plots are made on each model's submitted grid, i.e. they show the statistics before interpolation to the 1° grid. All statistics for all models are available in the ATLAS.

Neale and Hoskins (2000b) considered the response of a single model to these different SST fields. Here we determine how robust their results are by comparing 14 models.

3 Sensitivity to Meridional SST Profile

In this section we consider the changes in the simulations as the meridional profile of SST changes from the PEAKED case, in which the mid-latitude gradient continues to the equator, to the FLAT case, in which the equatorial maximum is very broad and SST is quartic in latitude, i.e. from PEAKED to CONTROL to QOBS to FLAT. In this sequence, the region of the primary SST gradient steepens, narrows, and moves poleward. For these four cases the SST is symmetric about the equator and the radiative forcing is symmetric about the equator. Thus the time average zonal means are also symmetric about the equator. Therefore we average the two hemispheres together to reduce the noise slightly and plot one hemisphere only, in the sense of the Northern Hemisphere. In addition, the abscissa adopts sine of latitude in order to provide detail in the tropical regions which exhibit more structure in many statistics.

3.1 Poleward Energy Transport

Blackburn et al. (2013) compared the insolation for APE to the annual average insolation for Earth. Since the SST is fixed, the fraction of insolation reaching the surface is lost. Nevertheless, an implied ocean poleward heat transport can be computed to balance the net surface energy flux if the global average energy imbalance is neglected. For each model the total poleward transport by the atmosphere plus an implicit underlying ocean has been computed to balance the net top of atmosphere (TOA) energy flux. These are averaged to give the APE multi-model mean transport. The implied oceanic component balances the net surface energy flux and the atmospheric component balances the difference between TOA and surface net fluxes. Globally averaged net fluxes have been removed and the two hemispheres have been averaged.

We first compare the poleward energy transport for the PEAKED, CONTROL, QOBS and FLAT experiments. The transports of the CONTROL were discussed in Blackburn et al. (2013) and compared to estimates of the annual average transport for Earth from Fasullo and Trenberth

(2008). Figure 2 shows the multi-model mean zonal-time average poleward energy transports for the four experiments (solid lines) along with the Fasullo and Trenberth (2008) estimates (dashed lines). Plus to minus one inter-model standard deviation is shaded. For each experiment, the atmospheric transport shows little variation between the APE models which are strongly affected by the fixed SST. This implies that the large range in the TOA net energy flux (not shown here, but available in the ATLAS and reflected in the total transport) passes through the atmosphere and affects the implied ocean transport.

The TOA net energy flux is relatively insensitive to SST. In the sequence from PEAKED to FLAT, the net downward flux increases slightly in the tropics and decreases in the extra-tropics. The decrease extends beyond the latitude of zero net flux near 40° which therefore shifts slightly equatorward. This leads to a small equatorward shift in the pattern of the total transport going from PEAKED to FLAT seen in Fig. 2, mainly associated with an increase in tropical transport. The equatorward shift brings the latitudinal distribution of the total transport closer to that of Earth although the overall amplitude increases at the same time so that the maximum total transport in the FLAT case is a little over 20% larger than that of Earth.

The TOA net energy flux and total poleward transport show almost no variation through the SST sequence poleward of 60° latitude where in all cases the SST fields are flat and equal to 0 C. In this region APE atmospheric and implied oceanic transports in Fig. 2 also show little variation through the SST sequence. The total transport is stronger than that of Earth, ultimately driven by the stronger gradient of insolation, but the atmospheric transport is less than that of Earth and the oceanic is larger. This is consistent with the APE lower boundary being open ocean with SST set to 0 C, which results in the APE atmosphere gaining more energy from the underlying surface than does Earth's atmosphere.

In mid-latitudes, changes in the atmosphere-ocean transport partition are broadly consistent with changes in the underlying SST gradient, shown in Fig. 1. In the PEAKED case, the atmosphere transport is weak and the ocean transport strong compared to the other cases, consistent with the weaker mid-latitude SST gradient, since the fixed temperature difference between the equator and 60° is linear in latitude. Between CONTROL and FLAT the changes are smaller. The atmosphere transport moves slightly poleward and strengthens, along with the maximum SST gradient, mainly by strengthening the poleward flank of the transport peak.

The most dramatic response of the atmosphere-ocean transport partition to SST occurs in the tropics. The total transport increases only slightly going from PEAKED to FLAT, but a broader tropical SST maximum produces weaker transport in the atmosphere and stronger

transport in the ocean equatorward of 30°. The QOBS case is closest to Earth, particularly for the atmosphere transport, with the total (and ocean) transport being slightly larger than observed. The change in transport partition with SST is so strong that, in the deep tropics for the PEAKED case, the atmosphere transports more energy than the total with equatorward transport in the ocean, while for the FLAT case the entire transport is carried by the ocean. The absence of poleward atmospheric transport in the deep tropics in the FLAT case is a first indication that the Hadley circulation does indeed break down in the APE models for this SST profile, as predicted by the theoretical model of Held and Hou (1980), leaving the atmosphere close to radiative-convective equilibrium at each latitude in the deep tropics.

The modest sensitivity of total poleward transport in the tropics to SST is due to a large degree of compensation between changes in net shortwave and longwave fluxes at the TOA in the tropics (shown in the ATLAS). In contrast, changes in net shortwave flux at the surface dominate over those in longwave and are augmented by changes in the turbulent heat fluxes, dominated by the latent heat flux. These contributions lead to the large opposing changes in separate atmosphere and implied ocean poleward transports. As the tropical SST maximum broadens going from PEAKED to FLAT, the net solar flux at the TOA and surface, which is downward, increases in the equatorial region and decreases in the subtropics, due to migration of deep cloud from the equator to the subtropics. The maximum surface latent heat flux similarly migrates poleward from the deep tropics in PEAKED to beyond 20° in FLAT. The reduction in near equatorial latent heat flux in the FLAT case is associated with weaker surface winds, again indicative of a breakdown of the large scale overturning circulation. The weaker evaporation more closely balances local precipitation (shown later), also indicating approximate radiative-convective equilibrium in the deep tropics. The maximum latent heat flux is influenced by both wind strength and the latitudinal gradient of saturated specific humidity, $q^*(T_S)$, so remains on the poleward flank of the subtropical trade winds. The large downward net surface flux at the equator in the FLAT case leads to the strong implied ocean transport.

Overall, all the transports in QOBS are most like those of Earth, with the atmosphere component being remarkably close.

3.2 Zonal Mean State

In this section we discuss how the multi-model mean simulated state changes as the meridional SST profile changes for the four zonally and hemispherically symmetric experiments. Blackburn et al. (2013) compared the CONTROL experiment with the Earth's climate. We first consider

the time average, zonal average precipitation for the individual models and for the multi-model mean. This provides an overview of the inter-model variability. We then consider the time average, zonal average of the three-dimensional atmosphere by examining the multi-model mean. Finally we describe the variation between the models and summarize it by showing the inter-model standard deviation of the zonal-time averages. The multi-model mean includes all models except FRCGC and UKMO(N96) as indicated in Table 1.

3.2.1 Precipitation

The zonal average, time average precipitation provides a good overview of the response of the Hadley circulation to changes in the SST profile. Figure 3 shows the zonal average total precipitation for the multi-model mean and for the individual models for the PEAKED, CONTROL, QOBS and FLAT experiments. The top two rows focus on the tropics, 0° to 25° latitude, where most of the response in precipitation occurs. The bottom two rows show the sub-tropics and extra-tropics, 15° to 90° latitude, with an enlarged precipitaton scale. To make the curves of the individual models more visible they are divided across two panels (e.g. first and second row) for each experiment (columns). The multi-model mean (over all models) is included on both panels of the pair.

Considering first the multi-model mean, the tropical precipitation maximum becomes weaker and broader from PEAKED to QOBS. It remains a single peak on the equator through the first three experiments, although it is basically flat within 5° latitude of the equator in QOBS. In the FLAT case the peak moves off the equator to around 14° latitude giving a wide double structure with symmetric peaks about the equator.

The PEAKED SST distribution yields a single ITCZ in all models, but the maximum precipitation rate varies greatly between models, by almost a factor of three. The FLAT case yields a pair of precipitation maxima symmetric about the equator in all models except LASG which retains a single but very weak maximum on the equator. In most models the off-equator maxima result in a clear double structure. The AGU has a secondary maximum on the equator which is almost as large as the off-equator peak values. Three other models (ECM-CY29, DWD and UKMO) also have a weak but notable peak on the equator, but the magnitude is appreciably less than the off-equator peak. These minor equatorial peaks are more easily seen in plots included in the ATLAS which contains individual figures for each model with graphs of the four experiments superimposed, the complement of Fig. 3. In the FLAT case the location of the maximum precipitation varies from 5° to 17° latitude in the different models. Through the

SST sequence PEAKED to FLAT, the double structure occurs first with the CONTROL in the CGAM, NCAR and UKMO-N48 models. It occurs first with QOBS for most of the remaining models and occurs first with FLAT in AGU, DWD and K1JAPAN. Thus all models except those last three show a double structure with QOBS yet the multi-model mean does not. The single structure of the multi-model mean is broad and relatively flat near the equator. The widely varying meridional structure seen in individual models is averaged out in the multi-model mean. The inter-model variability seen in the figure is quite striking with QOBS. The CONTROL has a fair amount of variability as well, but it is not as striking as QOBS since the maximum precipitation even when a double structure forms, occurs closer to the equator.

It is conceivable that averaging the two hemispheres as done here could hide the existence of a single off-equator structure which would be interpreted in the average as a weaker double structure. We have verified that this is not the case in any of the models in any of the experiments. It is also conceivable that the 3-year mean is not representative, due to possible intermittent switching between single and double structures in QOBS. We believe the 3-year mean is representative, but this cannot be guaranteed for all models since the APE protocol requested only a single 3-year average. Tests with the NCAR model preliminary to the APE design indicated that the structures were very stable and even single year averages showed no such intermitency. The single versus double structure is also stable for each model in four sequential 3-monthly averages of precipitation taken from the one-year of 6-hourly data, although the intensity varies as expected for such short samples.

In the multi-model mean, the secondary precipitation maximum associated with mid-latitude baroclinic waves, seen in the bottom two rows of Fig. 3, moves poleward through the SST sequence. The strength is very similar for PEAKED through QOBS then decreases slightly in FLAT. The largest shift in position occurs from QOBS to FLAT. As will be seen below, this is consistent with the poleward shift of the westerly jets and the baroclinic region. The individual models show a minor variation in the latitude and value of the mid-latitude maximum in PEAKED, CONTROL and FLAT. QOBS shows the largest variation in latitude and value of the maximum associated with the storm tracks.

Even though the maximum SST is the same in all cases, there is large variation in the maximum precipitation rate, and by inference in the maximum strength of the Hadley circulation, between the four experiments for a single model. (This is more obvious in Figures in the ATLAS which combine the four experiments into a single plot for each individual model.) Although the maximum precipitation rate varies greatly between the models and decreases through the se-

quence of SST fields, the tropical average shows much less variation. Figure 4 shows the time average tropical precipitation, averaged from -27° to $+27^\circ$ latitude, for the multi-model mean (bars) and inter-model standard deviation (whiskers at the top of the bars). The region is basically that shown in the top two rows of Fig. 3. The latitude boundaries were chosen around the minimum precipitation of the FLAT case (bottom two rows of Fig. 3) to separate the tropical precipitation from the extra-tropical. The other cases have a clearer separation between the tropics and mid-latitude precipitation with a very flat structure poleward of the ITCZ until the mid-latitude cell begins to form.

The average precipitation of the multi-model mean increases rather uniformly through the sequence from PEAKED to FLAT, from 3.40 to 4.21 mm/day, or by a little more than 20%. The increases CONTROL−PEAKED, QOBS−CONTROL and FLAT−QOBS are 0.34, 0.17 and 0.30 mm/day, respectively. All individual models (not shown) have a similar variation with SST, except for a small number in which average precipitation does not increase from QOBS to FLAT, giving the largest inter-model standard deviation for FLAT−QOBS. The increase is most likely associated with an increasing latitudinal extent of the tropical overturning circulation in the sequence PEAKED to FLAT that is evident in the zonal average vertical and meridional velocities in Fig. 5 and discussed in section 3.2.3. A broader tropical circulation provides a larger surface area of radiative cooling that is balanced predominantly by increased latent heating equatorward of 27° latitude.

These precipitation behaviors reaffirm for many models the discussion of Neale and Hoskins (2000b) from their single model result that the response to the SST is not a local thermodynamic one. There is a strong interaction between the formation of the convective maximum and the large-scale circulation. As will be seen below a strong precipitation maximum is accompanied by an intense vertical branch of the mean meridional circulation.

The widths of the convective maxima appear to depend on the near-equator curvature of the SST. The large near-equator gradient of the PEAKED gives a strong narrow single ITCZ. Weaker gradients (CONTROL, QOBS) lead to a wider single or double structure depending on the model. The FLAT with the weakest near-equator gradient leads to double structure with peaks relatively far from the equator with most models. This change in structure should be reflected in the dynamical variables discussed in the following sections.

In the FLAT case, Neale and Hoskins (2000b) describe the convection maxima in the HadAM3 model to be more a result of the interaction with mid-latitude systems than a pure ITCZ. In that case the greater baroclinicity leads to more intense troughs which trigger convec-

tion over the warmer waters which extend further poleward in the FLAT case. Other models, however, have different characteristics. Examination of animations of surface pressure and precipitation reveals that in many models the precipitation along this high latitude ITCZ has the character of tropical cyclones rather than hybrid tropical-extratropical disturbances in most models. In these models the precipitation band in the FLAT case is a type of ITCZ.

Of the specified SST, QOBS is the closest to the boreal winter profile in the Pacific. The transition from single to double ITCZ is seen to occur around the QOBS and CONTROL experiments. In addition QOBS shows the greatest variation in precipitation between models. Thus accurate tropical simulation of Earth may be particularly difficult to achieve. In addition, the mid-latitude storm tracks also show the largest variation between models with QOBS.

3.2.2 Zonal Wind and Temperature

We now consider the vertical and horizontal structure of the model responses to the SST profile, first examining the multi-model mean. The inter-model variability is discussed in the following section. The first row of Fig. 5 shows the temperature for the CONTROL and differences between successive experiments in the sequence PEAKED to FLAT. Through this sequence, SST warms most in the subtropics, decreasing the gradient in the tropics while increasing and shifting poleward the maximum extratropical gradient. These changes are mirrored through the depth of the troposphere, with low-level warming over the SST extending upwards in a band that tilts poleward with height and amplifies up to around 400 hPa. The response is largest for QOBS to FLAT. The second row of Fig. 5 shows that the westerly jet moves poleward through the SST sequence, with the latitude of the maximum value occurring at 27°, 30°, 32° and 46° latitude. The jet core strengthens slightly from 59 m $\sec^{-1}$ in the PEAKED to 62 m $\sec^{-1}$ in the CONTROL then weakens to 49 m $\sec^{-1}$ and 39 m $\sec^{-1}$ in QOBS and FLAT, respectively. The shift in the jet location is consistent with the poleward shift and weakening of the mid-latitude precipitation maximum seen earlier in Fig. 3. Although the jet shifts poleward along with the extratropical SST gradient, it weakens as the SST gradient strengthens. Two ingredients contribute to this counter-intuitive result. For the large poleward shift from QOBS to FLAT, the increase in Coriolis parameter acts to weaken the thermal wind by 25%, but this cannot account for a similar weakening of the jet for the much smaller shift from CONTROL to QOBS. Key to these changes is the latitude and tilt of the tropospheric warming relative to the existing jet. The tilt displaces the warming poleward of the maximum SST increase, which is generally equatorward of the jet. For PEAKED to CONTROL the tropospheric warming

is beneath the PEAKED jet, so its tilt gives approximately cancelling changes in temperature gradient (and thermal wind) in the lower and upper troposphere. The jet strengthens slightly with little poleward shift. For both CONTROL to QOBS and QOBS to FLAT the warming is displaced poleward of the jet, so the temperature gradient beneath the jet is reduced throughout the troposphere and the jet weakens. For QOBS to FLAT the accompanying large increase in temperature gradient on the poleward flank of the jet leads to the large poleward shift.

In contrast to the jet maximum in the upper troposphere, the mid-latitude surface westerlies strengthen monotonically and the maximum moves poleward from 32° to 45° latitude through the SST sequence, more closely related to the changes in mid-latitude SST gradient. Using aqua-planet simulations with a greater range of SSTs, Lu et al. (2010) suggest that the sensitivity of the surface westerlies to increasing SST gradient may be related to low level static stability on the equatorward flank of the jet, via its role in baroclinic growth rates. Certainly, in Fig. 5 the poleward-tilted temperature differences between the APE SST experiments do act to increase static stability in this manner, reducing baroclinic growth rates in the sub-tropics. Since the surface winds must be maintained against friction (the surface stress), the strengthening of the surface wind requires increasing momentum forcing by baroclinic eddies in the storm-track through the SST sequence. The upper tropospheric jet maximum is located equatorward of the surface westerlies in all but the FLAT experiment, indicating that the tropical overturning circulation is important in maintaining the jet in these cases. For FLAT the maximum westerly wind is vertically aligned, indicating the dominance of mid-latitude eddy forcing, with the tropical circulation playing a much smaller role on its sub-tropical flank.

Equatorial easterlies increase in strength and width through the SST sequence, with an additional closed contour forming below the tropopause in the FLAT experiment. The region of weak easterlies in the polar region deepens and narrows.

3.2.3 Meridional Circulation

The third and fourth rows of Fig. 5 show the meridional velocity and pressure vertical velocity respectively. In the multi-model mean, the mean meridional circulation shifts slightly poleward and weakens through the sequence PEAKED to QOBS. The continuing change to the FLAT is more dramatic. In the FLAT case the upward branch of the Hadley cell moves well off the equator to 12° latitude and equatorward flow forms in the equatorial region at 200 hPa. The transition to a double structure well off the equator by the FLAT SST is consistent with the theoretical model of Held and Hou (1980). However, as discussed below, the inter-model

variation in this transition is significant. In the sequence PEAKED to FLAT the maximum poleward flow at 200 hPa moves poleward from 6° to 8° to 10° to 18° latitude and decreases in strength from 4.2 to 3.9 to 3.1 to 1.4 m sec^{-1}. The maximum equatorward flow at the surface also moves poleward from 6° to 8° to 10° to 21° latitude and decreases in strength from -5.2 to -4.8 to -4.0 to -2.9 m sec^{-1}. The tropical upward branch of the Hadley cell decreases in strength from -178 to -102 to -54 to -22 hPa/day and in the FLAT case moves off the equator to 12° latitude. In the FLAT case a downward cell forms in the upper troposphere on the equator corresponding to the equatorward and easterly flow there. The omega field generally mirrors the multi-model mean precipitation seen earlier in Fig. 3 as expected. A strong precipitation maximum is accompanied by an intense vertical branch of the mean meridional circulation. The meridional velocity in the PEAKED experiment shows weak but noticeable shallow return flow at the equator at 700 hPa and equatorward flow at 400 hPa below the outflow at the top of the Hadley cell. This structure in the shallow return flow is present but weaker in the CONTROL experiment, insignificant in the QOBS, and absent in the FLAT.

The poleward edge of the Hadley circulation can be defined as the boundary between the equatorward and poleward flow at the surface. This boundary shifts to higher latitudes through the SST sequence and seems related to the shift in the ITCZ. This behavior is consistent with the angular momentum constraint on the size of the Hadley cell (Satoh, 1994). The shift of the ITCZ and poleward migration of the edge of the Hadley cell vary in the same way among the models as can be seen in plots for the individual models in the ATLAS.

3.2.4 Relative Humidity

The relative humidity is shown in the fifth (continued) row of Fig. 5. To a large extent the relative humidity reflects the changes in the mean meridional circulation. The relative humidity is maximum in the upward branch of the Hadley cell and minimum in the downward branch. As the circulation weakens through the SST sequence the relative humidity becomes more neutral decreasing in the upward branch and increasing in the downward branch of the Hadley cell. The minimum relative humidity shifts poleward also following the circulation. In the FLAT case the relative humidity contours become flat in the tropics reflecting the minimal Hadley circulation there. There is a slight local maximum in the region of weak upward motion around 12° latitude.

3.3 Variation Between Models

In this section we discuss the variation between the models that make up the multi-model mean zonal-time average. We consider two types of variability: the inter-model standard deviation for each individual SST experiment, and the inter-model standard deviation in the response to changes in SST shown in Figures 6 and 7, respectively. We do not show the many figures of zonal averages of the individual models. These are all available in the ATLAS. Also included there are plots of the individual models minus the multi-model mean, and the individual model differences for PEAKED−CONTROL, QOBS−CONTROL and FLAT−CONTROL.

3.3.1 Variability in Each SST Experiment

The inter-model standard deviation of the CONTROL is discussed in Blackburn et al. (2013). Figure 6 shows that there are common features in all experiments. We do not repeat all the details of the Blackburn et al. (2013) discussion here. Rather we concentrate on the differences associated with the changed SST.

For each experiment, in the troposphere the inter-model standard deviation of the zonal wind (Fig. 6, Row 2) increases with height as does the mean wind speed. It is maximum on the flanks of the jet where the maximum wind gradients occur and has a relative minimum near the jet axis. This pattern of inter-model variability is generally due to a poleward or equatorward shift of the maximum wind gradients in the individual models rather than to a widening or narrowing of the individual jet structures. The standard deviation increases markedly from PEAKED to CONTROL to QOBS, with strong variability in QOBS extending downward throughout the troposphere. The variability then decreases going to the FLAT SST, but the variability continues to extend throughout the troposphere. The North-South variability pattern of maximum, minimum, maximum also shifts poleward through the SST sequence following the shift of the jet axis.

The inter-model standard deviation becomes very large in the lower stratosphere, above 150 hPa. As discussed for the CONTROL in Blackburn et al. (2013), this is due to the very different behaviors of the lower stratosphere jet in the models, with some models extending the tropospheric jet into the stratosphere, some closing off the tropospheric jet to form a well separated stratospheric jet, and a few forming a very weak stratospheric jet. A similar situation arises with all the SST configurations. As mentioned in Blackburn et al. (2013), the lower stratospheric jet in these models is controlled by the top boundary conditions chosen for the

models. Thus the behavior there might be thought of as a computational artifact rather than being related to an attempt to model the local phenomenon and the variability reflects different modeling choices.

For each experiment the inter-model standard deviation of temperature (Fig. 6, Row 1) generally increases with height. There is strong increase in the mid-latitude and polar regions below the tropopause reaching a maximum at the tropopause reflecting large variability in the structure of the tropopause. This region of maximum inter-model variability shifts poleward and shrinks laterally in the sequence PEAKED to FLAT. As the region of extra-tropical variability shifts poleward, QOBS and FLAT develop a region of maximum variability below the tropical tropopause at the top of the upward branch of the Hadley cell. This is a reflection of different tropopause temperatures and thus of different gradients leading up to the tropopause. The tropical tropopause itself shows even stronger variability due to the strength and height of the tropopause in different models. The largest inter-model variability occurs in the tropical lower stratosphere, a region with large vertical gradient. There are also several model outliers contributing to this feature.

At each level in the troposphere, except near the surface, there is a local maximum which occurs equatorward of the region of maximum latitudinal temperature gradient before the temperature contours flatten going to the equator. The variability arises from differences in the vertical structure of the temperature there. This variability strengthens and shifts poleward through the SST sequence from PEAKED to QOBS then weakens slightly to FLAT. In the CONTROL, QOBS and FLAT there is a relative upper level maximum close to the jet core, collocated with the local minimum in variability in the zonal wind. Throughout the troposphere the largest variability is in the subtropics in the PEAKED and CONTROL but it spreads into the equatorial region in QOBS and FLAT.

The most notable feature in the inter-model variability of the mean meridional circulation is the large standard deviation associated with the upward branch of the Hadley cell (Fig. 6, Row 4). In PEAKED, CONTROL and QOBS the largest variability is on the equator with a secondary maximum on the poleward edge of the upward branch of the multi-model mean. This variability is primarily a reflection of the different strengths and depths of the upward motion in the different models, with the width and/or a single versus double structure making a secondary contribution. The single versus double plays a larger role in the variability in the QOBS as might be expected from the earlier discussion associated with the precipitation shown in Fig. 3 for the different models. In the FLAT case the center of the upward motion varies from the equator

to 15° latitude in the different models. The majority of models have the maximum around 15° latitude but with different strengths yielding the variability there, but a few place the maximum closer to the equator giving the secondary peak of variability at 5° latitude. The two peaks centered at 5° and 15° are primarily due to the variability in amplitude in the different models. A secondary contribution is introduced by slight differences in the location of the center of the individual model cells.

In the mid-latitudes the inter-model standard deviation of pressure vertical velocity increases from PEAKED to QOBS. It tends to occur in the transition region from downward to upward motion in the multi-model mean and reflects a shift in the latitude of transition in the different models. The mid-latitude inter-model variability decreases from QOBS to FLAT as the multi-model mean circulation becomes weaker.

For all SST distributions, the inter-model variability in the meridional velocity is greatest around the 200 hPa outflow region at the top of the Hadley cell (Fig. 6, Row 3). However, it extends below the outflow region, particularly in the PEAKED and CONTROL. In the outflow region itself the variability is due to variation in the strength of the Hadley cell. Below the outflow region the variability is primarily due to large variation in the strength of the secondary equatorward cell, although a few models have a deeper outflow region extending further down into the troposphere and a few others have a lower top to the Hadley cell. There is a cell of maximum inter-model variability associated with the surface flow into the Hadley cell. The variability strengthens from PEAKED to QOBS as the multi-model mean strength decreases. This variability is due to differences in the strength, depth and center of the inflow region. Variation in the secondary cell, or low level return flow contributes to the equatorial variability above 800 hPa which generally defines the top of the inflow region.

The upper troposphere shows a relative maximum in the inter-model variability in the meridional velocity in mid-latitudes. This variability increases from PEAKED to QOBS and is due to variation in the strength of the equatorward flow there. The variability in the FLAT case there is also primarily a variability in strength. The variability near the surface in mid-latitudes also increases from PEAKED to QOBS. This is also due to variation in strength, but it does not mirror the cell structure of the multi-model mean because the variation in the latitude of the cells also contributes to the variability.

The pattern of the standard deviation of the relative humidity seen in Blackburn et al. (2013) for the CONTROL changes little between the SSTs (Fig. 6, Row 5). However, the peak in the standard deviation at the sub-tropical inversion decreases through the SST sequence and shifts

poleward following the migration of the Hadley cell. This variability reflects differences in the inversion height and strength between models. This local maximum in the standard deviation occurs in the lower part of the downward branch of the Hadley cell with all SST distributions where the multi-model mean has the largest downward motion, especially in PEAKED and CONTROL. Although the variability is primarily associated with a large inter-model variability in specific humidity, a relative maximum variability in temperature also contributes. The decrease through the SST sequence reflects a decrease in the moisture difference across the inversion seen in the multi-model mean (Fig. 5, Row 5) where FLAT is moister in the free troposphere.

Inter-model variability in the upward branch of the Hadley circulation increases with height reaching a relative maximum around 300 hPa at the top of the region of strong upward motion. The varibility increases through the sequence and spreads poleward as the Hadley cell broadens. Continuing upward, after a local minimum, the variability reaches a further maximum at the tropical hygropause, the level of minimum water vapor mixing ratio. This maximum varies little with SST reflecting the fact that this sharp feature remains at a fixed height determined by deep tropical convection. In contrast, the relative humidity standard deviation peak at the polar hygropause decreases through the sequence as the polar hygropause rises. The inter-model variability in relative humidity through the polar troposphere is related more to the variability in temperature than to the variability in specific humidity. The variability is similar for the four SST fields.

In all the fields, QOBS exhibits the largest inter-model variability, not only in the tropical Hadley cell but also in the region of the extra-tropical jet.

3.3.2 Variability in response to changes in SST

In this section we consider the inter-model standard deviation of the response to the changed SST, i.e. the standard deviation in the differences EXPERIMENT−CONTROL. We note again that, as seen in the ATLAS, there are 3 or 4 models that are relative outliers that can lead to anomalously large inter-model standard deviations in some regions. This can negate the utility of the standard deviation in those regions. Nevertheless, we retain the philosophy of including all models in the analysis. In affected fields, we try to flag those regions where the standard deviation is less meaningful.

In general, as can be seen in the ATLAS, the individual model difference fields EXPERIMENT−CONTROL for a given field have similar structures. The primary difference

between models response to the changed SST is in the amplitude of these structures. However, shifts in the basic patterns also contribute to the inter-model variability, but they appear to be of secondary importance.

The first row of Fig. 7 shows the inter-model standard deviation of EXPERIMENT−CONTROL for the temperature. The largest variability in temperature in QOBS−CONTROL and FLAT−CONTROL is below and above the tropical tropopause. However that inter-model variability is due to a single outlier (LASG) and is uninformative. The significant variability is in the extra-tropics extending into the tropics. The core of the maximum closely follows that of the pattern of the EXPERIMENT−CONTROL differences for the multi-model mean (Fig. 5, row 1), especially in the PEAKED case. The maximum inter-model variability in the difference is shifted equatorward of the maximum in the multi-model mean difference in the other two cases. The patterns do not match the inter-model standard deviation of the individual experiments (Fig. 6, row 1). The implication is that the strength of the responses to the changes in SST differs, while the patterns of the changes are similar even though there is significant variability in the individual structures between models for any one experiment.

The inter-model standard deviation of EXPERIMENT−CONTROL for the zonal wind is shown in the second row of Fig. 7. Concerning the mid-latitude jet, the difference, PEAKED−CONTROL shows little variability among the models. On the other hand, the QOBS−CONTROL and FLAT−CONTROL show significant variability among the models. The inter-model variability in the upper tropical tropopause, particularly in FLAT−CONTROL, is associated with the difference in the extension of the westerlies into the tropics.

The inter-model variability in the meridional wind for the three SST differences is shown in Fig. 7, row 3. The upper tropical tropopause variability is due to variability of the changes in the strengths of the outflow at the top of the Hadley cell and of the changes in the secondary inflow just below. The variability near the surface is due to variability of the changes in the strength and to variability of the shifts of the centers of cells of poleward and equatorward flow.

The inter-model variability in the pressure vertical velocity (Fig. 7, row 4) for all three SST differences is primarily associated with the upward branch of the Hadley cell and mimics variability in the individual experiments. It is partly due to the change from single to double ITCZ, which occurs at different places in the SST sequence with different models, and partly to different changes in strength in individual models with changes in the SST even when the basic structure does not change.

Figure 7, row 5 shows the inter-model variability in the change in relative humidity as the

SSTs are changed. The larger variability in the PEAKED−CONTROL in the lower troposphere around 20° to 30° latitude is associated with different shifts of the poleward edge of the subsidence region where the relative humidity gradient is large. In the plots of the differences for the individual models themselves in the ATLAS, the inter-model differences in the minimum and maximum relative humidity on the equatorward and poleward sides, respectively, catch the eye. However the slight shift in the latitudinal gradient of relative humidity introduces more variability and this dominates the inter-model differences in Fig. 7. The relative humidity variability between 30° and 40° latitude in QOBS−CONTROL and in FLAT−CONTROL is also due primarily to the differences in the shift in location of the gradient as the subsidence region moves poleward. The variability around 20° latitude in QOBS−CONTROL is due to differences in the minimum relative humidity in the subsidence region itself. The equatorial variability in the relative humidity difference mimics that of the upward branch of the Hadley cell seen in vertical velocity.

From the individual model plots in the ATLAS there are indications (but no more) of a relationship between tropical and extra-tropical responses to the SST profiles. This is related to the ITCZ regime change near QOBS. Models in which the ITCZ splits before QOBS have a stronger poleward shift of the mid-latitude jet between the CONTROL and QOBS. In addition, those models in which the split ITCZ is located closer to the equator have a weaker shift in the FLAT case relative to the CONTROL.

3.4 Maintenance of zonal mean state

3.4.1 Transient eddies

Figure 8 shows the multi-model mean and inter-model standard deviation transient eddy momentum $\overline{[u'^* v'^*]}$ and heat fluxes $\overline{[v'^* T'^*]}$ for the four SST fields. Following generally accepted notation, the overbar $\overline{(\ )}$ denotes the time average, prime ($'$) denotes the deviation from the time average, square brackets [ ] denote the zonal average and star (*) denotes the deviation from the zonal average. The transient eddy poleward heat flux (third row) strengthens as the SST shifts from PEAKED to FLAT and the center moves poleward. The poleward momentum flux (first row) strengthens while the equatorward flux weakens, both in the polar and equatorial regions. The poleward momentum flux shifts poleward in parallel with the jet core shifting poleward. The individual models all show qualitatively the same variation from PEAKED to FLAT but there is significant variability in the strength of the cells for any one experiment

as seen in Blackburn et al. (2013) for the CONTROL experiment. The inter-model standard deviations reflect that variability.

3.4.2 Parameterized thermodynamic forcing

Seven models submitted the total parameterized heating for all experiments. This is the sum of the radiation, turbulence or planetary boundary layer (including the surface sensible heat flux), convection and large scale condensation. Figure 9 shows the zonal averaged total parameterized heating for a selection of 4 of those models, AGU, ECM-CY32, K1JAPAN and NCAR. The fields are plotted on the individual model vertical and horizontal grids. We do not calculate a multi-model mean of the parameterization components because they can be highly dependent on the vertical grid and important details can be lost by vertical interpolation to a common grid. This might be less of an issue with the total shown in Fig. 9, but even there some layer structures are apparent. The particular models shown in Fig. 9 are chosen to illustrate the variety of behaviors in the models. The parameterized heating for all models can be seen in the ATLAS. Of those not included here, UKMO(N48) resembles ECM-CY32 but without the break in the heating around 600 hPa. ECM-CY29 also resembles ECM-CY32 but the heating in QOBS associated with the upward branch of the Hadley cell moves off equator, consistent with double ICTZ structure in ECM-CY29. The pattern in GSFC is somewhat similar to AGU but the heating is significantly stronger in GSFC and it has a layer at 800 hPa where the heating becomes very small, possibly due to the evaporation of rain.

In all models, the heating in the tropics becomes weaker through the sequence PEAKED to FLAT, with the heating in the FLAT case moving away from the equator. This is consistent with the weakening of the Hadley circulation seen earlier in the discussion of the zonal mean meridional circulation in Section 3.2.3. It is also consistent with the variation in precipitation discussed in Section 3.2.1.

Of course, the tropical heating, vertical motion and precipitation are all intimately related. The tropical heating in the PEAKED and CONTROL experiments are rather similar to each other in all models with larger differences between the models going from CONTROL to QOBS. In NCAR there is a slight cooling in QOBS on the equator in the upper troposphere indicative of the more widely spaced double structure in precipitation. Cooling also occurs in ECM-CY29 (not shown) while ECM-CY32 shows the double structure, but with heating at the equatorial minimum. In the FLAT experiment, AGU has no structure in the heating in the tropics. The other models all show weak heating associated with upward motion. K1JAPAN keeps the

heating near the equator with no cooling on the equator. In the other models (ECM-CY29, GSFC, and UKMO(N48), not shown) the heating maximum in the FLAT case occurs poleward of 10° latitude as seen in Fig. 9 for ECM-CY32 and NCAR. The cooling around 800 hPa in the subsidence region, which is primarily from longwave radiation, decreases through the sequence, more so in those models with strong cooling there in the CONTROL (ECM-CY29, ECM-CY32, and UKMO(N48)) than those with modest cooling. The large variability in cooling between the models for a single SST field is due to differences in the low clouds. The heating in mid-latitudes in the baroclinic regions also decreases through the SST sequence in all models.

3.5 Tropical variability

3.5.1 Tropical waves

The temporal variability of tropical precipitation in the models may be quantified using wavenumber-frequency diagrams, following the analysis methodology of Wheeler and Kiladis (1999). A template for this analysis is shown in Fig. 10. It includes the conventional dispersion curves for the odd meridional mode-numbered equatorial waves of Matsuno (1966) and Gill (1980) for equivalent depths of 12, 25, and 50m (see Wheeler and Kiladis, 1999). The odd numbered modes correspond to divergence and temperature, and by assumption precipitation, that is symmetric about the equator. The U-shaped curves in the upper half of the plots show westward (WIG) and eastward (EIG) propagating inertio-gravity waves. The diagonal lines from bottom center to the right are eastward propagating Kelvin modes (KELVIN) and the lower curves from zero to the left are westward propagating equatorial Rossby waves (ER). In the following for convenience we refer to the types of mode based on their frequency signatures relative to the dispersion curves. However, we do not know if their spatial structures actually correspond to those types of the theoretical modes.

Figure 11 shows the log of the power of the symmetric component of the unnormalized spectra of the 6-hour averaged precipitation, averaged from 20°S to 20°N for selected models. The full power is plotted without removing a background spectrum in order to allow a comparison of the overall power of the waves as well as the wave characteristics. In the aqua-planet the wave characteristics emerge from the total without a normalization. The multi-model mean is not very informative for this statistic. Therefore, to save space, we have chosen to show only a few models to indicate the variety of behaviors seen among the models. All the models are shown in Blackburn et al. (2013) for the CONTROL experiment and in the ATLAS for all the

experiments. None of the models shown here are representative of other models which are not shown, those have even different behaviors. It is very difficult to find two models whose wave characteristics are similar through the sequence PEAKED to FLAT. In Blackburn et al. (2013) the wavenumber-frequency diagrams for the CONTROL show precipitation averaged from 10°S to 10°N. The domain is enlarged here because much of the tropical precipitation in the FLAT experiment moves poleward of 10° latitude (see Figure 3). For the experiments in which the precipitation remains within the 10°S to 10°N region, the effect of the larger domain is to reduce the average power somewhat but to retain the basic structure. This can be verified by comparing the relevant plots in the ATLAS or by comparing plots of the CONTROL here with those in Blackburn et al. (2013).

In Fig. 11 AGU has a relatively weak Kelvin mode signature in all experiments, decreasing in power through the sequence PEAKED to FLAT, reaching weak power in all modes by FLAT. The lack of power in the FLAT experiment is consistent with other aspects seen earlier in the AGU model of very weak tropical activity even though the zonal average tropical precipitation is similar to many other models (Fig. 3). The AGU model tends to have its power in the equatorial Rossby modes, particularly in the CONTROL and QOBS. Differences between the two ECM versions are noteworthy. Major revisions were made to the convective parameterization in ECM-CY32 (Bechtold et al., 2008). This pair in particular illustrates the importance of the interaction between the dynamics and the parameterizations. The dynamical core and resolution are the same in the two cycles. ECM-CY29 has weaker Kelvin waves through the SST sequence, with almost none in the FLAT experiment. ECM-CY32 also has minimal power in the Kelvin modes in the FLAT experiment. In the PEAKED and CONTROL, the power of the ECM-CY29 modes tends to be independent of wavenumber and to depend on the period with the contours being rather horizontal except for a modest Kelvin wave signature. The power of the ECM-CY32 modes, on the other hand, tends to follow the dispersion curves, and decreases with increasing wavenumber. Both versions develop equatorial Rossby waves in the QOBS and FLAT experiments. In the QOBS ECM-CY29 has relatively more power in the equatorial Rossby modes compared to the Kelvin modes, while ECM-CY32 has the opposite partition, with relatively more power in the Kelvin than in the equatorial Rossby modes. K1JAPAN retains Kelvin structure through the sequence to the FLAT experiment as does NCAR. In both models westward propagating equatorial Rossby modes strengthen through the sequence. Overall K1JAPAN has more power than NCAR but NCAR isolates the Kelvin modes more throughout the sequence.

Several models show a clear shift from eastward propagating Kelvin modes to westward propagating equatorial Rossby modes through the sequence PEAKED to FLAT. In addition to those shown in Fig. 11 are CGAM, CSIRO, DWD, GFDL, GSFC, LASG, MIT and UKMO(N48). All of that list, except GSFC, have almost no indication of Kelvin waves in the FLAT case, i.e. the pattern of the power is like that of ECM-CY29 in Fig. 11 but the power varies between models. Most of the models retain some power in the Kelvin modes in QOBS. Those that have very little are, in addition to AGU in Fig. 11, CSIRO and MIT.

Westward low frequency power is generally less dispersive than the equatorial Rossby modes, as noted by Blackburn et al. (2013) for the CONTROL experiment. This is likely to be a doppler shifting due to the presence of easterly zonal flow throughout the equatorial troposphere (Gui-Ying Yang, 2011, personal communication), as Fig. 5 shows is increasingly the case in the sequence PEAKED to FLAT. In the PEAKED experiment in ECM-CY29 and K1JAPAN there is significant westward power at low zonal wavenumbers on timescales of around 3 days that does not correspond to any of the symmetric equatorial modes. It is possible that this is associated with the anti-symmetric mixed Rossby-gravity mode leaking power into symmetric precipitation. The corresponding spatial structures are worthy of further investigation.

3.5.2 Tropical precipitation frequency distribution

Figure 12 shows the fraction of the time the precipitation is in each 1 mm day^{-1} bin ranging from 0 to 120 mm day^{-1}. The left-most bin is the fraction of time the precipitation is exactly 0, and the right-most bin the fraction of time the precipitation exceeds 120 mm day^{-1}. A gap in the curve indicates the fraction is zero for that bin. The fraction is computed for the 6-hour averaged precipitation over all points between 20°S to 20°N. Blackburn et al. (2013) discussed the frequency distribution for the precipitation averaged from 10°S to 10°N for the CONTROL. Since the precipitation moves poleward of that domain with almost all models for FLAT and with some models for QOBS we extend the region here. As can be seen by comparing plots of the CONTROL here with those in Blackburn et al. (2013) the effect is to reduce the fraction of large precipitation rates in the CONTROL, and by implication in the PEAKED and QOBS, since the region now includes more points with low precipitation amounts. Since the extreme precipitation rates are highly dependent on the model grid size (Williamson, 2008), the model grid data have been averaged to a 5 degree latitude-longitude grid before calculating the frequency distribution. Corresponding plots based on the original model grid values can be seen in the ATLAS. The general characteristics discussed below concerning the dependence on

the different SST fields for each model are qualitatively the same for the frequency distribution based on the model grid data, but the inter-model differences are significantly greater.

In general, there is a trend for a decrease in the fraction of large values through the sequence, along with a decrease in the largest values of precipitation themselves. For many models, PEAKED and CONTROL are very close to each other relative to the other SST distributions. For four models the difference in frequency distribution between the different SST distributions is very subtle (CGAM, LASG, MIT and NCAR). Of these CGAM and NCAR have relatively low maximum precipitation rates and LASG and MIT have very large maximum precipitation rates, on the order of 200 mm/day. (For the frequency distribution for all experiments which include a larger precipitation range see the ATLAS). Two models show significant gap between CONTROL and QOBS (ECM-CY29 and GFDL). ECM-CY29 and GFDL have large precipitation rates for the PEAKED and CONTROL experiments (400 and 200 mm/day, respectively) but both models decrease the precipitation rates substantially for the QOBS experiment.

4 Sensitivity to Off-Equatorial SST Maximum

The fifth zonally symmetric SST distribution (CONTROL_5N) shifts the maximum SST off the equator to 5°N latitude. It is intended primarily to examine the asymmetry in convection and the Hadley cell when the maximum SST is no longer centered on the equator. As discussed in the introduction, the theoretical model of Held and Hou (1980), when applied to a asymmetric SST profile by Lindzen and Hou (1988), gave a significantly more intense overturning circulation crossing the equator into the winter hemisphere than in the symmetric case, even for displacement of the temperature maximum by only a few degrees.

The CONTROL_5N SST is a distortion of the CONTROL SST created by shifting the maximum from 0° to 5°N latitude while continuing to have the SST go to 0C at both 60°N and 60°S latitudes. Thus the mid-latitude gradient is stronger in the Northern or "summer" hemisphere than in the Southern. This planet does not completely mimic the Earth which generally has an equatorial minimum in SST, particularly in the East pacific, giving two peaks in the SST profile. One might expect such a double peak to more easily drive a double ITCZ.

4.1 Zonal mean state

We first examine the response of the precipitation to the off-equatorial shift of the SST maximum. Figure 13 shows the zonal average, time average precipitation for the multi-model mean and for

the individual models plotted between 25°N and 25°S. In all models, the ITCZ moves off the equator in CONTROL_5N following the SST maximum. In many models the ITCZ weakens and broadens. In those models with broadening it occurs via a slightly larger shift of the precipitation into the Northern Hemisphere. Both these characteristics are visible in the multi-model mean plot. The weakening of the precipitation is balanced by the broadening to yield very similar tropical averages. The average from 25°N to 25°S of the multi-model mean increases by 0.1 mm/day from 3.9 mm/day for the CONTROL to 4.0 mm/day for CONTROL_5N. The inter-model standard deviation of the tropical average is 0.7 mm/day for both experiments. The inter-model standard deviation of the differences of the averages is 0.06 mm/day.

Most models that produce a single equatorial maximum in the CONTROL retain the single structure in the CONTROL_5N. The maximum remains single and moves off the equator clearly following the SST maximum to 5°N to within the resolution of the individual model grids. Recall, the individual model discrete grids might not have a grid point at 5°N nor be symmetric about 5°N. This single-ITCZ behavior dominates the multi-model mean. Two models with a single ICTZ in the CONTROL (ECM-CY29 and MIT) form a hint of a double ITCZ in CONTROL_5N, although these are very weak signals. In three of the models that had a double structure in the CONTROL (CGAM, NCAR and UKMO(N96)), the double structure moves with the SST in the CONTROL_5N, retaining the relative minimum over the maximum SST at 5°N. The southern maximum moves close to the location of the minimum in CONTROL at the equator. We again note that the symmetry of the structure may be compromised by the discrete sampling in the CONTROL_5N where the grid points are not necessarily symmetric about the SST maximum. One model (GSFC) which had a slight double structure in the CONTROL created a single structure in the CONTROL_5N.

Figure 14 shows the zonal average u, v and omega for the multi-model mean for the CONTROL and CONTROL_5N experiments. As consistent with the precipitation, the upward branch of the Hadley circulation moves off the equator in CONTROL_5N following the SST maximum. All three fields indicate that the southern hemisphere Hadley cell dominates. The cross-equatorial cell is stronger with a wider region of descent. However, the asymmetry of the overturning circulation and low level easterly trade winds in the APE multi-model mean is much more modest than in both the theoretical and idealised numerical models of Lindzen and Hou (1988).

Neale and Hoskins (2000b) report that in their experiments with the Met Office HadAM3 model two distinct ascent maxima appear with the lower troposphere one closer to the equator.

They attribute this behavior to two distinct convective maxima, the lower close to the equator and the higher over the region of maximum SST. Here, the multi-model mean shows only a hint of such structure with a horizontal separation of about 1 grid point (on the 1° interpolation grid) and a barely discernible upper maximum. In fact only a few of the models develop such a double structure, namely CSIRO, GSFC and MIT (not shown), and thus it does not appear in the multi-model mean. The individual models are not shown here but plots are included in the ATLAS. The individual model total parameterized temperature tendencies (not shown here but also included in the ATLAS) tend to support the presence or lack of double vertical structure in the vertical velocity for those models which submitted the parameterization terms.

4.2 Tropical waves

With the formation of equatorial asymmetries in the CONTROL_5N experiment the natural question is: Is there a shift in the power of the tropical waves from symmetric to anti-symmetric modes compared to the CONTROL? We find it difficult to discern any systematic shift in power from symmetric to anti-symmetric modes in the wavenumber-frequency plots for the individual models. The plots are available in the ATLAS but not included here because the signal, if any, is extremely weak. There are, perhaps, subtle shifts for some models, but these are very subjective, difficult to discern by eye, and other investigators may draw a different interpretation. For the precipitation, a few appear to have a slight decrease of power in symmetric modes and an increase in antisymmetric (GSFC, K1JAPAN, MRI and NCAR). Other models show little change (AGU, CGAM, CSIRO and MIT) and two indicate a decrease in anti-symmetric power (DWD and ECM-CY29). The power in the OLR shows even less shift from symmetric to antisymmetric, with all models but two being rather neutral, and two (AGU and DWD) showing, if anything, a decrease in power in the anti-symmetric modes in the CONTROL_5N case.

5 Summary

We have presented a selection of circulation statistics from the intercomparison of APE models for the five zonally symmetric SST fields originally specified by Neale and Hoskins (2000a). Four of these are hemispherically symmetric and labeled PEAKED, CONTROL, QOBS and FLAT. This SST sequence is designed to indicate the sensitivity of the Atmospheric General Circulation Models to the meridional SST profile. All SSTs have the same maximum at the equator but differ in their meridional gradients approaching the equator. They range from a strong SST

gradient continuing to the equator (PEAKED) to a flat approach to the equator with maximum gradient poleward of 20° latitude. The fifth SST is a hemispherically asymmetric modification of the CONTROL, with the maximum SST shifted to 5°N. Denoted CONTROL_5N, it is designed to examine the response when the maximum SST is not on the equator. Here we are able to present only a small sample of the multitude of statistics that have been calculated and are available in the ATLAS (Williamson et al., 2012). Simulations from the CONTROL are described in greater detail in Blackburn et al. (2013).

The general sensitivity to the changed SST is illustrated by the response in multi-model mean statistics. The variability of the individual model responses is quantified by the inter-model standard deviation. In fact, the most striking feature in these experiments is the large variation between models, both within a single experiment and in the response to changes in SST. Thus the multi-model mean should not be considered as a best estimate of the aqua-planet climate. It is simply a convenient way to generalize the sensitivities of the current set of AGCMs. In this set, no one model is a good match for the multi-model mean. All models differ significantly in many fields from the multi-model mean. This was particularly apparent in the tropics with QOBS where the multi-model mean precipitation indicated a single ITCZ yet all but three models produce a double ITCZ with differing strengths and widths.

For precipitation we include line plots of the zonal average for all the individual models to indicate the nature of the inter-model variability. For multi-level fields we present the multi-model mean and the inter-model standard deviation of the zonal average. Space does not allow inclusion of contour plots of the zonal averages for all models. In this case the salient features which contribute to the inter-model standard deviation are described verbally. Plots for all models are available in the ATLAS. Some statistics, for which a multi-model mean is awkward, are shown here for selected models only, with the intent of illustrating the range of behaviors among the models rather than being all inclusive.

For the symmetric SST profiles, the APE models confirm the expectation from the theoretical model of Held and Hou (1980) and a number of idealised numerical model studies, that the tropical overturning circulation undergoes a regime transition as the tropical SST profile is flattened in the sequence PEAKED to CONTROL to QOBS to FLAT. The symmetric Hadley circulation, with a single ITCZ and rising motion on the equator, that occurs for the PEAKED equatorial SST profile, breaks down for the FLAT SST profile which has quartic variation with latitude. The resulting circulation consists of a pair of widely spaced ITCZs and overturning circulations directed poleward into the sub-tropics. This leaves the deep tropics much closer

to radiative-convective equilibrium at each latitude, with weak circulation and uniform weak precipitation.

The general trend, to weaken the Hadley circulation and shift it poleward as the SST profile flattens, is clearly evident in the overturning circulation in the multi-model mean, and to different degrees in the precipitation of all individual models. The details, however, vary greatly between models. All the models form a single ITCZ at the equator with the PEAKED SST. A few models form a double ITCZ structure on the equator for the CONTROL SST and most form a double ITCZ with QOBS, even though, as described above, a double structure does not appear in the multi-model mean. In almost all the models, the ITCZ is widely split for the FLAT SST, with a relatively weak ITCZ poleward of 10° latitude. In contrast, the double ITCZ for CONTROL and QOBS remains close to the equator in most models, with significant precipitation on the equator. However, in a few models, the ITCZ is almost completely split in QOBS, indicating that the double ITCZ seen in many AGCM simulations is related to the regime transition with SST profile. Of the specified SSTs, QOBS is the closest to the boreal winter Eastern Pacific profile. The transition from single to double ITCZ is seen to occur around the QOBS experiment and this SST also shows the largest inter-model variability. This result implies that accurate tropical simulation of Earth may be particularly difficult to achieve.

Even though the maximum SST is the same in all experiments, there is large variation between models in the change in the precipitation with different equatorial SST gradients, and a large variation between the individual models for any one SST. The response to the SST is not a local thermodynamic one. There is an important interaction between the formation of the convective maximum and the large-scale circulation.

The mid-latitude jet core moves poleward over the sequence of SST from PEAKED to FLAT. The jet strengthens slightly from PEAKED to CONTROL, then weakens to QOBS and FLAT. In contrast, mid-latitude surface westerlies increase monotonically and the maximum moves poleward. Equatorial easterlies increase in strength and the region of easterlies widens. This pattern is seen in all models, but the magnitude of the changes differ by more than a factor of two among the models. The transient eddy poleward heat flux strengthens as the SST shifts from PEAKED to FLAT and the center moves poleward. The poleward momentum flux strengthens and shifts poleward while the equatorward flux weakens. Again the inter-model variability of these eddy transports and transport changes is significant.

The tropical wave characteristics are also very different among the models for all SST distributions. In general, however, the tropical wave activity tends to decrease going from CONTROL

to QOBS to FLAT although the details of the changes are very different for the different models. The partition of power between classes of equatorial wave mode also changes through the sequence. Eastward propagating Kelvin modes tend to be predominant in many models with the sharper equatorial SST gradients but reduce in power with the reduction in SST gradient, particularly from QOBS to FLAT. This indicates that the precipitation in widely spaced off-equator ITCZs projects weakly onto the equatorially peaked divergence structure of the Kelvin mode. Westward propagating equatorial Rossby waves, on the other hand, tend to increase in power with the reduction in SST gradient. Once again, this is a general assessment but there is a large inter-model variability with exceptions to the above description. Such vastly different behaviors illustrate further the importance of the interaction between the dynamics and the parameterizations.

The tropical precipitation frequency distribution was also considered. In general all models show a decrease in the fraction of large values through the SST sequence PEAKED to FLAT, along with a decrease in the largest values of precipitation themselves. However, both the magnitude of the changes and where in the SST sequence the most notable changes occur, vary greatly among models, as do the frequency distributions themselves for any one SST distribution.

We then examined the sensitivity to off-equatorial SST maximum, i.e. the change from the CONTROL to the CONTROL_5N SST distributions. In the multi-model mean, the upward branch of the Hadley circulation follows the SST maximum off the equator into the Northern Hemisphere and the center of the precipitation maximum remains centered over the SST maximum. Those models that have a relatively strong double ICTZ in the CONTROL experiment also form one in the CONTROL_5N with minimum precipitation remaining over the shifted SST maximum. However, one model that has a very weak double structure in the CONTROL forms a single in the CONTROL_5N and one that has a single structure in the CONTROL, forms a double in CONTROL_5N. Most models show a reduction in the maximum value of precipitation in the CONTROL_5N, no model shows an increase. The weakening of the maximum precipitation is balanced by a broadening of the structure such that the tropical average precipitation increases marginally. With the upward branch of the Hadley circulation moving into the Northern Hemisphere the zonal average u, v and omega all indicate that the southern hemisphere Hadley cell dominates.

However, the asymmetry of the overturning circulation and low level easterly trade winds in the APE multi-model mean is much more modest than in both the theoretical and idealised numerical models of Lindzen and Hou (1988). Again, the variation between the individual

models is large. Since the CONTROL_5N SST introduced equatorial asymmetries into the simulations it is natural to ask if there a shift in the power of the tropical waves from symmetric to anti-symmetric modes. We were unable to identify such a systematic shift from the wavenumber-frequency plots.

The aqua-planet presents a much more constrained experimental environment than earth-like simulations such as AMIP (Gates, 1992; Gates et al., 1999). Nevertheless, a repeating theme is the large variability among the models for each single SST experiment and the large variability in the responses of the models to changes in the specified SST. These variations are perhaps smaller than found in AMIP but nevertheless are significant. We have concentrated primarily on statistics responding to the parameterized moist processes and their interaction with the resolved dynamics. In the companion paper describing results from the CONTROL, Blackburn et al. (2013) also discuss aspects that are more constrained and therefore have less variation between models.

In the APE models, resolution undoubtedly influences the interaction between the resolved dynamical flow and the parameterized moist processes. Many of the APE models have relatively coarse resolution, so that baroclinic waves do not fully develop. In a baroclinic instability test case Jablonowski and Williamson (2006) show that, in the set of models they examined, spectral truncation of T85, or grid resolution of 1 degree was needed to capture the baroclinic growth of eddies. In the NCAR CAM, Williamson (2008) has shown that, even for longitudinal wavenumbers less than 15, T170 truncation is required to obtain convergence in the tropical wave characteristics. Many of the APE models were applied at lower resolutions and thus different truncation errors in the dynamical component can play a significant role in the inter-model variability.

As with most intercomparison projects involving earth-like AGCMs it is difficult to determine the cause of the differences in the model behaviors. Now the issue is to understand the causes of the different model responses. That requires further exploratory experiments, formation of hypotheses and experiments to verify or refute the hypotheses. We hope the Aqua-Planet Experiment will stimulate researchers to do just that, and that it provides a significantly simpler environment to explore the differences that have been exposed by the intercomparison. The APE simulations are freely available from the APE web site (http://climate.ncas.ac.uk/ape/) and we encourage researchers to perform more thorough analyses of individual phenomena than we have been able to do here. We also hope that as new models are developed they will repeat the APE simulations.

6 Acknowledgments

We thank two anonymous reviewers whose comments helped to improve the manuscript. Richard Neale (NCAR), Peter Gleckler (Program for Climate Model Diagnosis and Intercomparison, PCMDI) and staff at PCMDI contributed to the APE diagnostic specification, data protocol and initial collection and quality control of the data. Williamson was partially supported by the Office of Science (BER), U.S. Department of Energy, Cooperative Agreement No. DE-FC02-97ER62402. He thanks J. Olson for carrying out the NCAR APE simulations. The National Center for Atmospheric Research is sponsored by the National Science Foundation. Bechtold and Wedi thank J.J. Morcrette and M. Hortal for their help in setting up the ECMWF/IFS simulations. Stratton thanks Chris Dearden for his help in reformatting and transferring the output from the Met Office simulations to PCMDI. Contributions from the Met Office are Crown Copyright. McGregor thanks Martin Dix for his assistance. The numerical calculation of AFES was carried out on the Earth Simulator under support of JAMSTEC.

References

Bechtold, P., M. Köhler, T. Jung, F. Doblas-Reyes, M. Leutbecher, M. J. Rodwell, F. Vitart, and G. Balsamo, 2008: Advances in simulating atmospheric variability with the ECMWF model: From synoptic to decadal time-scales. *Quart. J. Roy. Meteor. Soc.*, **134**, 1337–1351.

Blackburn, M. and B. J. Hoskins, 2013: Context and aims of the Aqua-Planet Experiment. *J. Meteor. Soc. Japan*, **91A**, this issue, doi:10.2151/jmsj.2013-A01.

Blackburn, M., D. L. Williamson, K. Nakajima, W. Ohfuchi, Y. O. Takahashi, Y.-Y. Hayashi, H. Nakamura, M. Ishiwatari, J. L. McGregor, H. Borth, V. Wirth, H. Frank, P. Bechtold, N. P. Wedi, H. Tomita, M. Satoh, M. Zhao, I. M. Held, M. J. Suarez, M.-I. Lee, M. Watanabe, M. Kimoto, Y. Liu, Z. Wang, A. Molod, K. Rajendran, A. Kitoh and R. Stratton, 2013: The Aqua-Planet Experiment (APE): CONTROL SST simulation. *J. Meteor. Soc. Japan*, **91A**, this issue, doi:10.2151/jmsj.2013-A02.

Butler, A. H., D. W. J. Thompson, and T. Birner, 2011: Isentropic slopes, downgradient eddy fluxes, and the extratropical atmospheric circulation response to tropical tropospheric heating. *J. Atmos. Sci.*, **68**, 2292–2305.

Fasullo, J. T. and K. E. Trenberth, 2008: The annual cycle of the energy budget. part II: Meridional structures and poleward transports. *J. Climate*, **21**, 2313–2325.

Gates, W. L., 1992: AMIP: The Atmospheric Model Intercomparison Project. *Bull. Am. Met. Soc.*, **73**, 1962–1979.

Gates, W. L., et al., 1999: An overview of the results of the Atmospheric Model Intercomparison Project (AMIP I). *Bull. Amer. Meteor. Soc.*, **80**, 29–55.

Gill, A. E., 1980: Some simple solutions for heat-induced tropical circulation. *Quart. J. Roy. Meteor. Soc.*, **106**, 447–462.

Hayashi, Y.-Y. and A. Sumi, 1986: The 30-40 day oscillations simulated in an "Aqua Planet" model. *J. Meteor. Soc. Japan*, **64**, 451–467.

Held, I. M. and A. Y. Hou, 1980: Nonlinear axially symmetric circulations in a nearly inviscid atmosphere. *J. Atmos. Sci.*, **37**, 515–533.

Hess, P. G., D. S. Battisti, and P. J. Rasch, 1993: Maintenance of the intertropical convergence zones and the large-scale tropical circulation on a water-covered earth. *J. Atmos. Sci.*, **50**, 691–713.

Jablonowski, C. and D. L. Williamson, 2006: A baroclinic instability test case for atmospheric model dynamical cores. *Quart. J. Roy. Meteor. Soc.*, **132**, 2943–2975.

Liang, X.-Z. and W.-C. Wang, 1996: Atmospheric ozone climatology for use in General Circulation Models. http://www-pcmdi.llnl.gov/projects/amip/AMIP2EXPDSN/OZONE/OZONE2/o3wangdoc.html, Atmospheric Sciences Research Center, State University of New York at Albany.

Lin, J.-L., 2007: The double-ITCZ problem in IPCC AR4 coupled GCMs: Ocean-atmosphere feedback analysis. *J. Climate*, **20**, 4497–4525.

Lindzen, R. S. and A. V. Hou, 1988: Hadley circulations for zonally averaged heating centered off the equator. *J. Atmos. Sci.*, **45**, 2416–2427.

Lorenz, D. J. and E. T. DeWeaver, 2007: Tropopause height and zonal wind response to global warming in the IPCC scenario integrations. *J. Geophys. Res.*, **112**, D10 119, doi:10.1029/2006JD008087.

Lu, J., G. Chen, and D. M. W. Frierson, 2010: The position of the midlatitude storm track and eddy-driven westerlies in aquaplanet AGCMs. *J. Atmos. Sci.*, **67**, 3984–4000.

Matsuno, T., 1966: Quasi-geostrophic motions in the equatorial area. *J. Meteor. Soc. Japan*, **44**, 25–43.

Neale, R. B. and B. J. Hoskins, 2000a: A standard test for AGCMs including their physical parameterizations. I: The proposal. *Atmos. Sci. Lett.*, **1**, 101–107, doi:10.1006/asle.2000.0022.

Neale, R. B. and B. J. Hoskins, 2000b: A standard test for AGCMs including their physical parameterizations. II: Results for The Met Office Model. *Atmos. Sci. Lett.*, **1**, 108–114, doi:10.1006/asle.2000.0024.

Pope, V. D., M. L. Gallani, P. R. Rowntree, and R. A. Stratton, 2000: The impact of new physical parametrizations in the Hadley Center Climate Model – HadAM3. *J. Climate*, **16**, 123–146.

Satoh, M., 1994: Hadley circulations in radiative-convective equilibrium in an axially symmetric atmosphere. *J. Atmos. Sci.*, **51**, 1947–1968.

Wang, W.-C., X.-Z. Liang, M. P. Dudek, D. Pollard, and S. L. Thompson, 1995: Atmospheric ozone as a climate gas. *Atmospheric Research*, **37**, 247–256.

Wheeler, M. C. and G. N. Kiladis, 1999: Convectively coupled equatorial waves: Analysis of clouds and temperature in the wavenumber-frequency domain. *J. Atmos. Sci.*, **56**, 374–399.

Williamson, D. L., 2008: Convergence of aqua-planet simulations with increasing resolution in the Community Atmospheric Model, Version 3. *Tellus*, **60A**, 848–862.

Williamson, D. L., M. Blackburn, B. J. Hoskins, K. Nakajima, W. Ohfuchi, Y. O. Takahashi, Y.-Y. Hayashi, H. Nakamura, M. Ishiwatari, J. L. McGregor, H. Borth, V. Wirth, H. Frank, P. Bechtold, N. P. Wedi, H. Tomita, M. Satoh, M. Zhao, I. M. Held, M. J. Suarez, M.-I. Lee, M. Watanabe, M. Kimoto, Y. Liu, Z. Wang, A. Molod, K. Rajendran, A. Kitoh and R. Stratton, 2012: The APE Atlas. Tech. Rep. NCAR/TN-484+STR, National Center for Atmospheric Research, xxii+508 pp. Available from the APE website http://climate.ncas.ac.uk/ape/ and to be made available from http://opensky.library.ucar.edu/search/?ky=technotes.

Yin, J. H., 2005: A consistent poleward shift of the storm tracks in simulations of 21st century climate. *Geophys. Res. Lett.*, **32**, L18 701, doi:10.1029/2005GL023684.

Figure Captions

Figure 1: Zonal average SST for PEAKED, CONTROL, QOBS, FLAT and CONTROL_5N, °C

Figure 2: Multi-model mean poleward energy transport for the PEAKED, CONTROL, QOBS and FLAT experiments (solid lines). Plus to minus one inter-model standard deviation is shaded. Total transport is that required to balance the top of atmosphere net radiative flux; ocean transport is that implied to balance the surface net flux; atmospheric transport is the difference between the two. Annual mean observational estimates for Earth are included for comparison, from Fasullo and Trenberth (2008) (dashed). Values shown are averaged over the Northern and Southern hemispheres.

Figure 3: Zonal average, time average total precipitation for multi-model mean and individual models from PEAKED, CONTROL, QOBS and FLAT SST distributions (mm day^{-1}). The top two rows include just the tropical region while the bottom two plot the extra-tropical region on a different scale.

Figure 4: Tropical-time average (-27° to +27°) precipitation for multi-model mean and standard deviation from PEAKED, CONTROL, QOBS and FLAT SST distributions (mm day^{-1})

Figure 5: Zonal-time average multi-model mean temperature (t), zonal wind (u), meridional wind (v), pressure vertical velocity (om) and relative humidity (rh) for PEAKED, CONTROL, QOBS and FLAT. Temperature plots are for differences between experiments as indicated above each column, except for the CONTROL itself which is contoured from 190 to 300 by 5 K.

Figure 6: Inter-model standard deviation of the zonal-time average for temperature (t), zonal wind (u), meridional wind (v), pressure vertical velocity (om) and relative humidity (rh) for PEAKED, CONTROL, QOBS and FLAT.

Figure 7: Inter-model standard deviation of the differences, experiment - control, of the zonal-time average for temperature (t), zonal wind (u), meridional wind (v), pressure vertical velocity (om) and relative humidity (rh) for PEAKED−CONTROL, QOBS−CONTROL and FLAT−CONTROL.

Figure 8: Multi-model mean and standard deviation, transient eddy momentum $\overline{[u'^* v'^*]}$ and heat fluxes $\overline{[v'^* T'^*]}$ for PEAKED, CONTROL, QOBS and FLAT.

Figure 9: Parameterized total temperature tendency for individual models for PEAKED, CONTROL, QOBS and FLAT, K day^{-1}.

Figure 10: Template of dispersion curves for wavenumber-frequency diagrams of symmetric equatorial modes shown in Fig. 11.

Figure 11: Wavenumber-frequency diagrams of log of power of symmetric modes of equatorial precipitation from AGU, ECM-CY29, ECM-CY32, K1JAPAN and NCAR for PEAKED, CONTROL, QOBS and FLAT, $-20°$ to $+20°$ latitude. The template for the dispersion curves is shown in Fig. 10.

Figure 12: Fraction of time that 6 hour averaged precipitation from $-20°$ to $+20°$ latitude is in 1 mm day^{-1} bins ranging from 0 to 120 mm day^{-1} for individual models for PEAKED, CONTROL, QOBS and FLAT experiments. Grid values have been conservatively averaged to a $5°$ latitude-longitude grid.

Figure 13: Zonal-time average precipitation for individual models from CONTROL and CONTROL_5N SST distributions, mm day^{-1}.

Figure 14: Zonal-time average multi-model mean u, v and omega for CONTROL (top) and CONTROL_5N (bottom).

Table 1: PARTICIPATING MODELS

	GROUP SYMBOL	LOCATION	MODEL	TUNED TOA?[1]	PCQF[3]	C5N[4]
1	AGU	Japan (consortium)	AFES	No	X	X
2	CGAM	Reading, UK	HadAM3	Yes	X	X
3	CSIRO	Aspendale, Australia	CCAM	No	X	X
4	DWD	Offenbach/Mainz, Germany	GME	Yes	X	X
5	ECM-CY29	Reading, UK	IFS cy29r2	No	X	X
6	ECM-CY32	Reading, UK	IFS cy32r3	No	X	
7	FRCGC	Yokohama, Japan	NICAM	No		
8	GFDL	Princeton, USA	AM2.1	Yes	X	X
9	GSFC	Maryland, USA	NSIPP-1	No	X	X
10	K1JAPAN	Japan (collaboration)	CCSR/NIES 5.7	Yes	X	X
11	LASG	Beijing, China	SAMIL	No	X	X
12	MIT	Cambridge, USA	MIT-GCM	No	X	X
13	MRI	Tokyo, Japan	MRI/JMA98	No	X	X
14	NCAR	Boulder, USA	CCSM-CAM3	Yes	X	X
15	UKMO(N48)	Exeter, UK	pre-HadGAM1	Weakly[2]	X	
16	UKMO(N96)	Exeter, UK	pre-HadGAM1	Weakly[2]		X

[1] i.e. was the top of atmosphere radiative balance optimised for present day Earth climate?
[2] During the development phase of HadGEM1 the TOA fluxes of AMIP runs were monitored to check that they did not widely diverge from balance but were not actively tuned.
[3] Submitted results from PEAKED, CONTROL, QOBS and FLAT experiments.
[4] Submitted results from CONTROL and CONTROL_5N experiment.

Table 2: DYNAMICAL PROPERTIES OF PARTICIPATING MODELS

GROUP SYMBOL	DYNAMICAL CORE	WATER VAPOR TRANSPORT	HORIZON RESOLUTION	VERT
AGU	Eulerian spectral	Eulerian spectral	T39	L48
CGAM	lat-lon grid point	Eulerian grid	3.75° x 2.5°	L30
CSIRO	C-C[1] semi-Lag[2]	semi-Lag	∼210 km (C48)	L18
DWD	icosahedral grid	semi-Lag grid	∼1°	L31
ECM-CY29	semi-Lag spectral	semi-Lag grid	T159	L60
ECM-CY32	semi-Lag spectral	semi-Lag grid	T159	L60
FRCGC	icosahedral Eulerian	Eulerian	∼7 km	L54
GFDL	lat-lon finite volume	finite volume	2.5° x 2°	L24
GSFC	lat-lon grid point	Eulerian centered	3.75° x 3°	L34
K1JAPAN	Eulerian spectral	semi-Lag grid	T42	L20
LASG	Eulerian spectral	Eulerian grid	R42	L9
MIT	cubed sphere	Eulerian grid	∼280 km	L40
MRI	Eulerian spectral	Eulerian spectral	T42	L30
NCAR	Eulerian spectral	semi-Lag grid	T42	L26
UKMO(N48)	semi-Lag lat-lon grid	semi-Lag	3.75° x 2.5°	L38
UKMO(N96)	semi-Lag lat-lon grid	semi-Lag	1.875° x 1.25°	L38

[1] C-C denotes conformal cubic, [2] semi-Lag denotes semi-Lagrangian

Table 3: PARAMETERIZATIONS OF PARTICIPATING MODELS

GROUP SYMBOL	PBL	SHALLOW CONVECTION	DEEP CONVECTION
AGU	Mellor-Yamada	None	Emanuel
CGAM	Smith	Gregory-Rowntree	Gregory-Rowntree
CSIRO	Holtslag-Boville	None	McGregor
DWD	Louis	Tiedtke	Tiedtke
ECM-CY29	Louis-Beljaars	Tiedtke	Bechtold et al. 2004
ECM-CY32	Louis-Beljaars	Bechtold et al. 2008	Bechtold et al. 2008
FRCGC	Mellor-Yamada	None	None
GFDL	Lock	RAS[1]	RAS
GSFC	Louis	RAS	RAS
K1JAPAN	Mellor-Yamada	None	Pan-Randall
LASG	Local vert diffusion	None	Manabe
MIT	Mellor-Yamada	RAS	RAS
MRI	Mellor-Yamada	Randall-Pan	Randall-Pan
NCAR	Holtslag-Boville	Hack	Zhang-McFarlane
UKMO(N48)	Lock/Richardson	Gregory 1990 /Grant	Gregory 1999
UKMO(N96)	Lock/Richardson	Gregory 1990 /Grant	Gregory 1999

[1] RAS denotes relaxed Arakawa-Schubert.

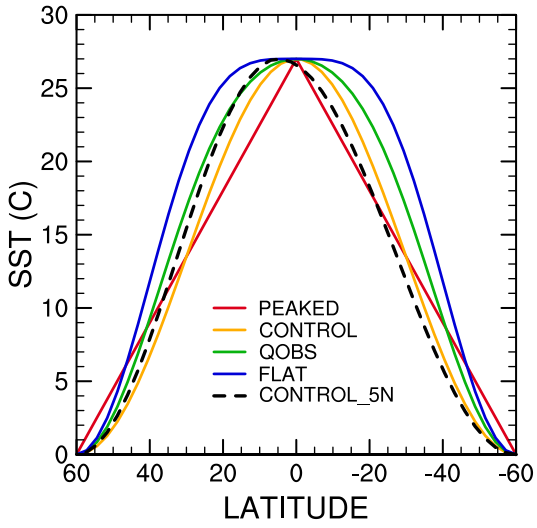

Figure 1: Zonal average SST for PEAKED, CONTROL, QOBS, FLAT and CONTROL_5N, °C

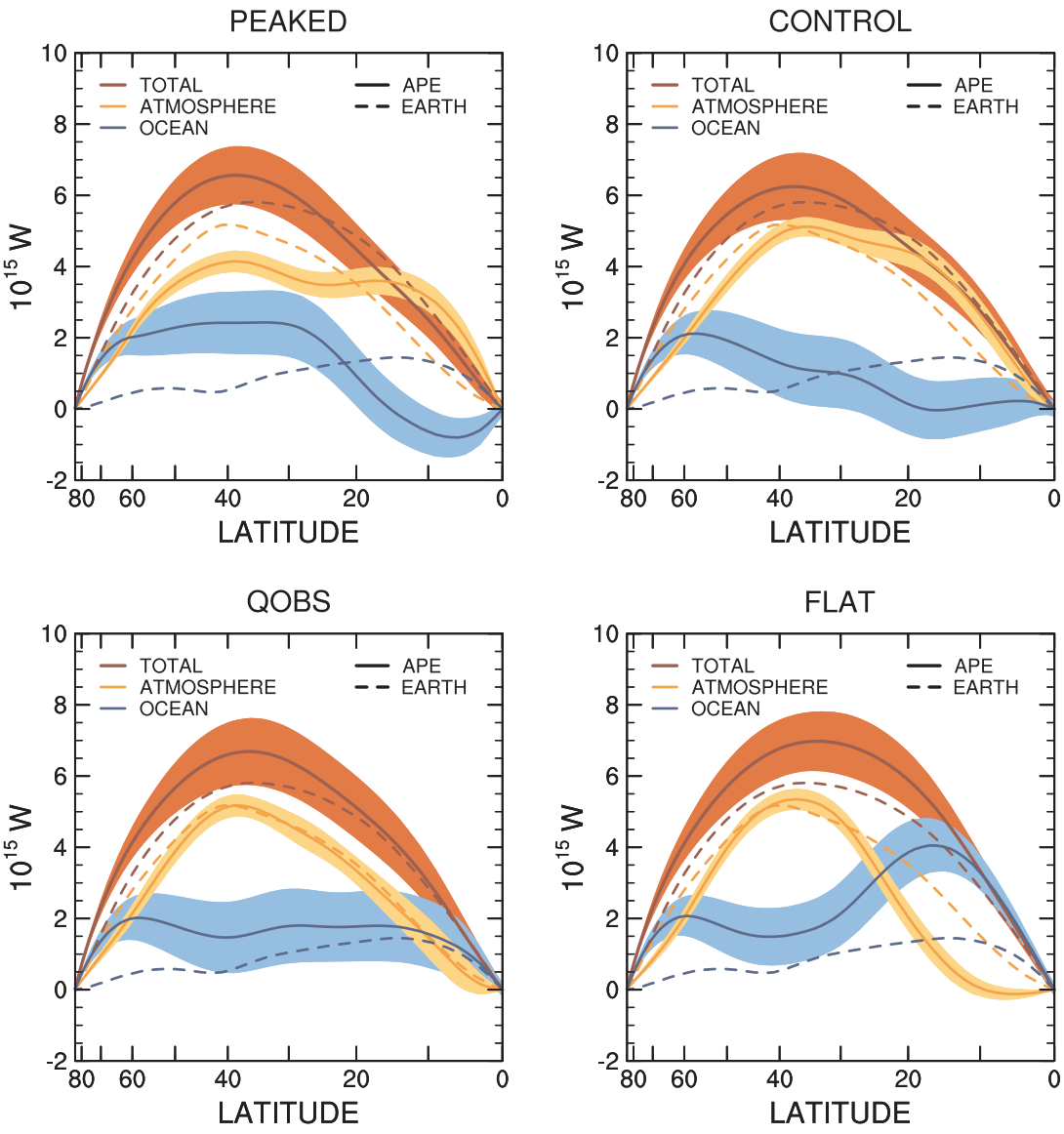

Figure 2: Multi-model mean poleward energy transport for the PEAKED, CONTROL, QOBS and FLAT experiments (solid lines). Plus to minus one inter-model standard deviation is shaded. Total transport is that required to balance the top of atmosphere net radiative flux; ocean transport is that implied to balance the surface net flux; atmospheric transport is the difference between the two. Annual mean observational estimates for Earth are included for comparison, from Fasullo and Trenberth (2008) (dashed). Averages of the two hemispheres are shown.

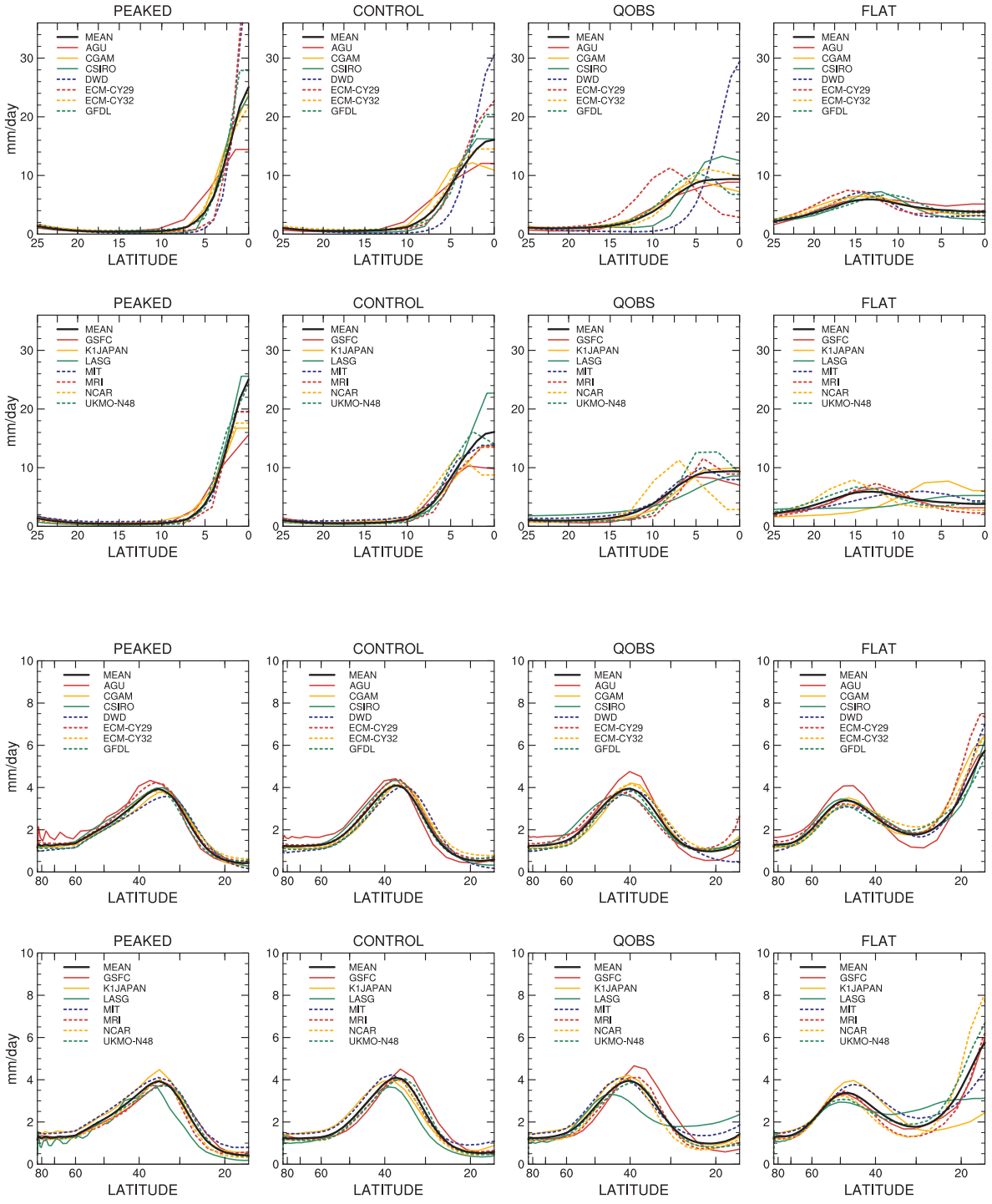

Figure 3: Zonal average, time average total precipitation for multi-model mean and individual models from PEAKED, CONTROL, QOBS and FLAT SST distributions (mm day^{-1}). The top two rows include just the tropical region while the bottom two plot the extra-tropical region on a different scale.

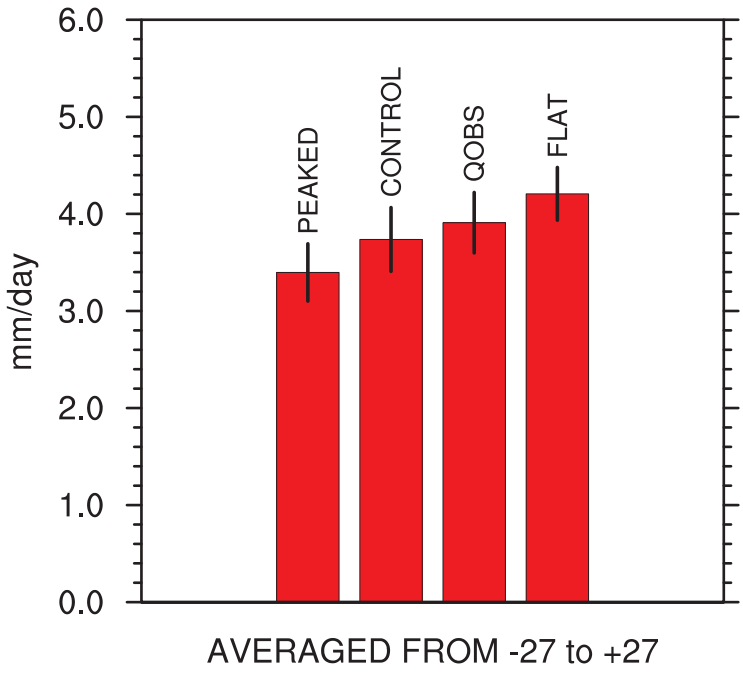

Figure 4: Tropical-time average (-27° to +27°) precipitation for multi-model mean and standard deviation from PEAKED, CONTROL, QOBS and FLAT SST distributions (mm day^{-1})

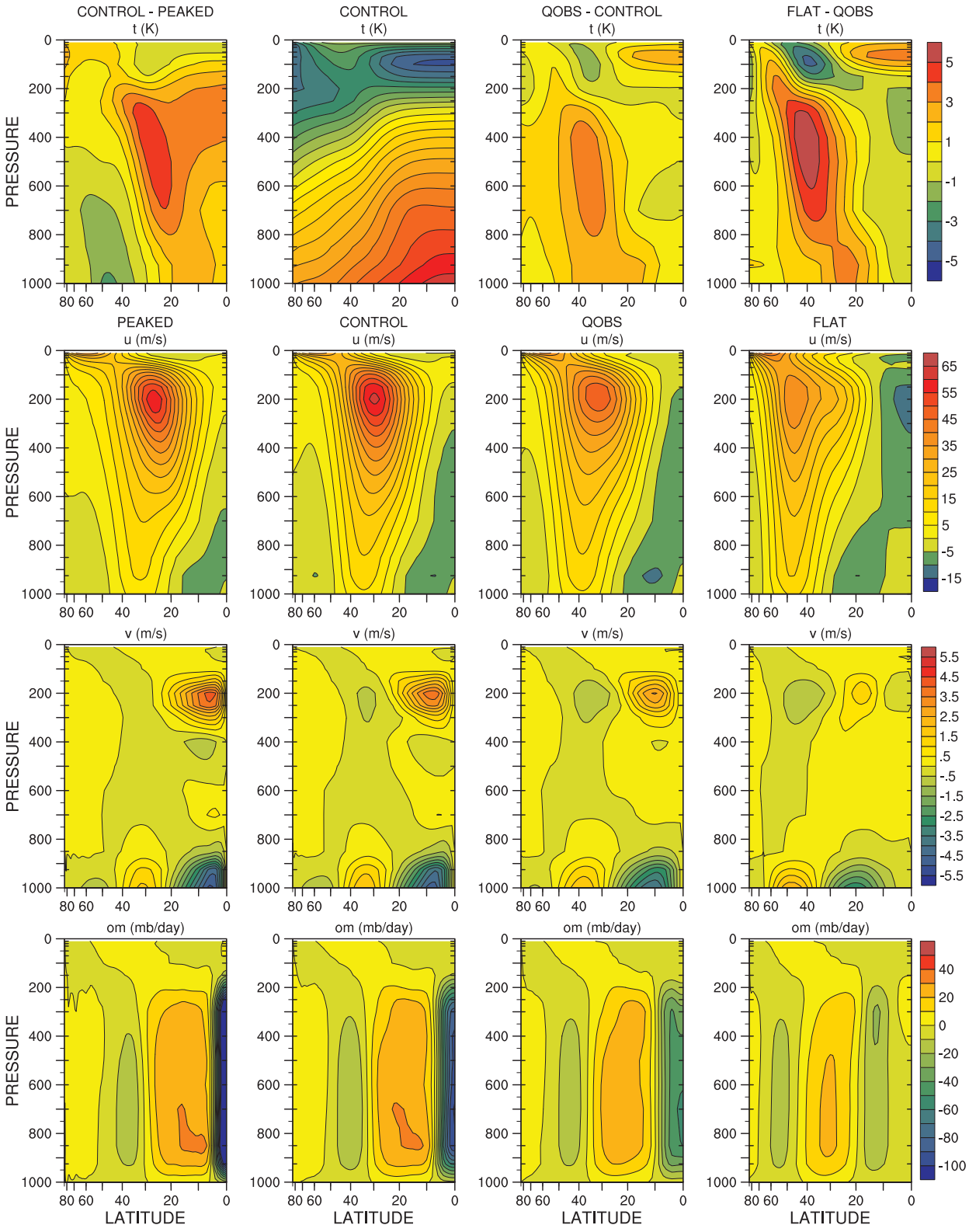

Figure 5: Zonal-time average multi-model mean temperature (t), zonal wind (u), meridional wind (v), pressure vertical velocity (om) and relative humidity (rh) for PEAKED, CONTROL, QOBS and FLAT. Temperature plots are for differences between experiments as indicated above each column, except for the CONTROL itself which is contoured from 190 to 300 by 5 K.

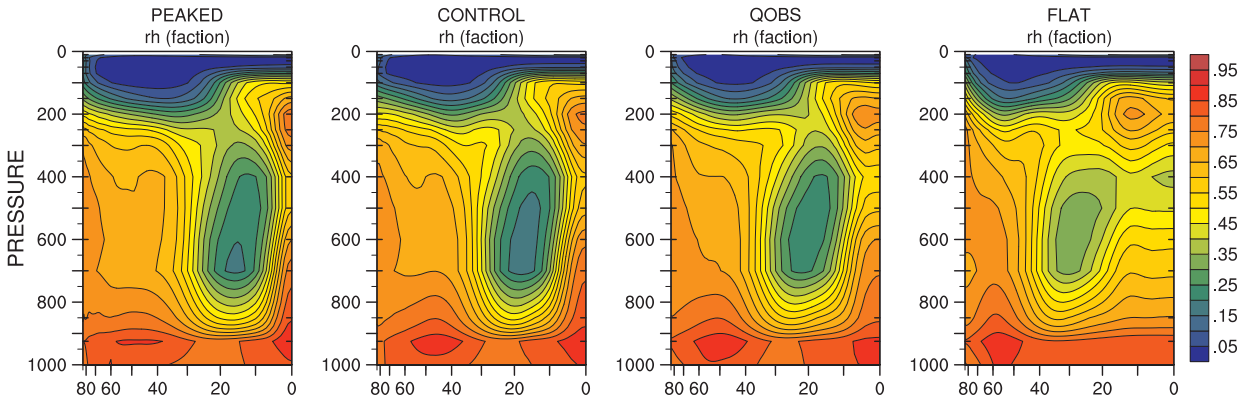

Figure 5 (continued): Zonal-time average multi-model mean temperature (t), zonal wind (u), meridional wind (v), pressure vertical velocity (om) and relative humidity (rh) for PEAKED, CONTROL, QOBS and FLAT. Temperature plots are for differences between experiments as indicated above each column, except for the CONTROL itself which is contoured from 190 to 300 by 5 K.

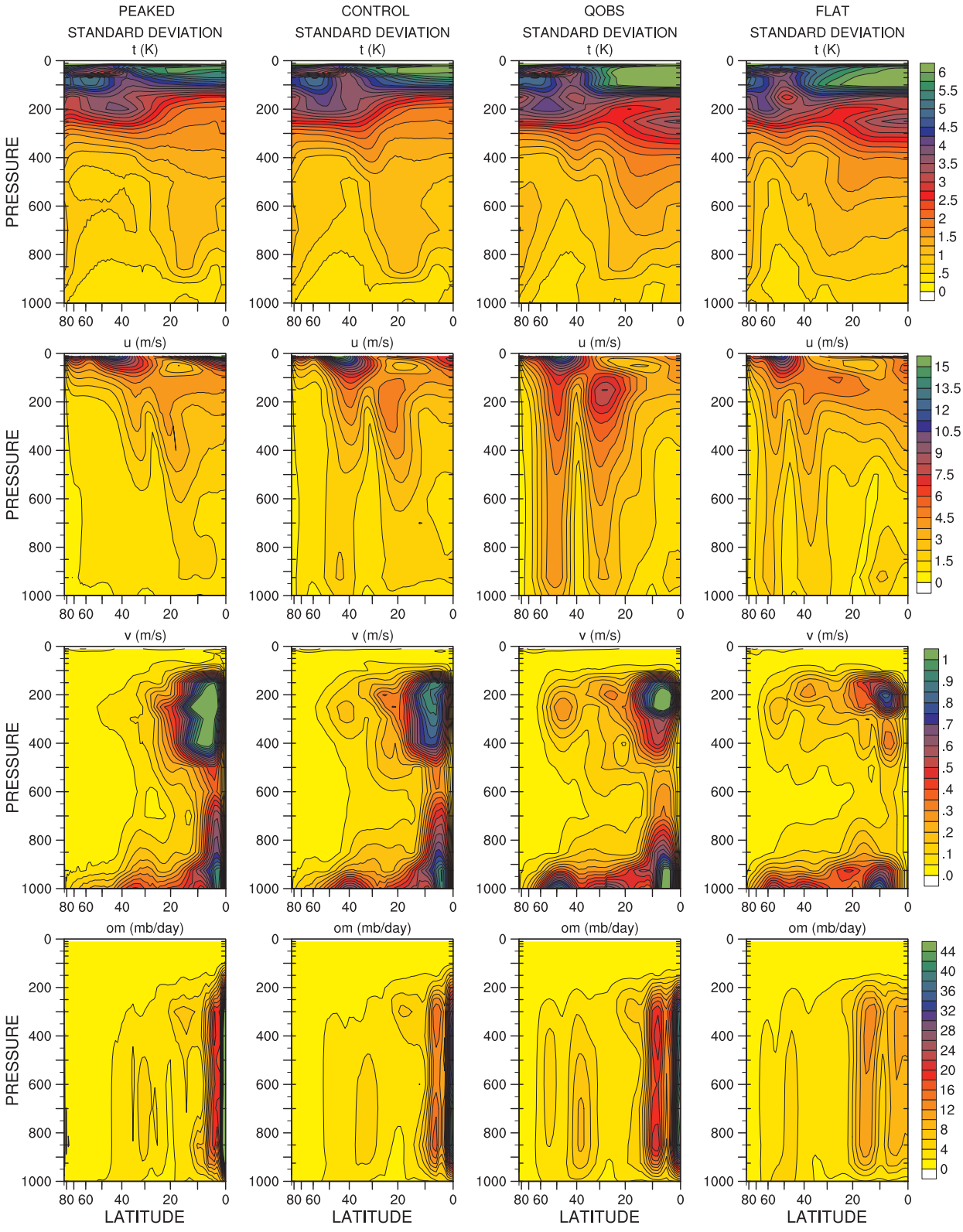

Figure 6: Inter-model standard deviation of the zonal-time average for temperature (t), zonal wind (u), meridional wind (v), pressure vertical velocity (om) and relative humidity (rh) for PEAKED, CONTROL, QOBS and FLAT.

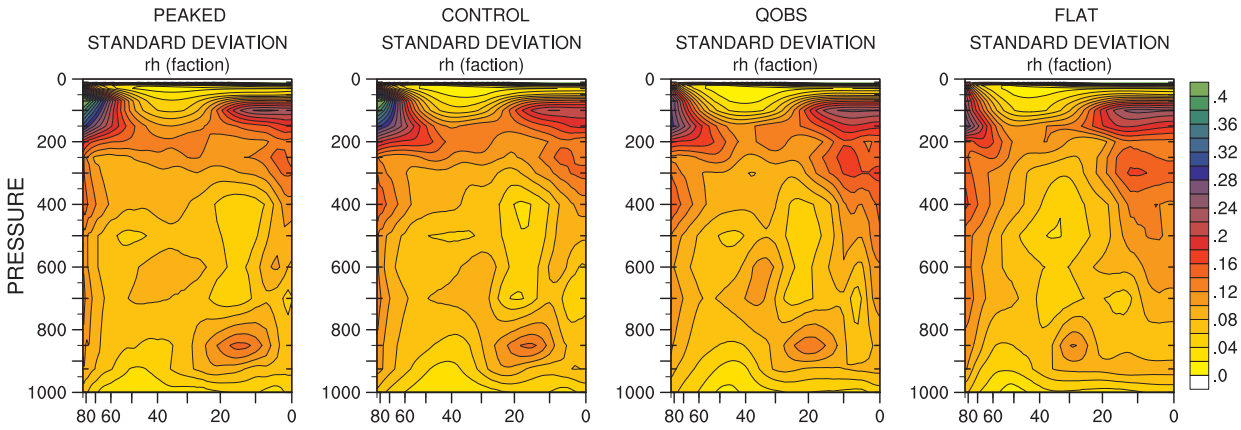

Figure 6 (continued): Inter-model standard deviation of the zonal-time average for temperature (t), zonal wind (u), meridional wind (v), pressure vertical velocity (om) and relative humidity (rh) for PEAKED, CONTROL, QOBS and FLAT.

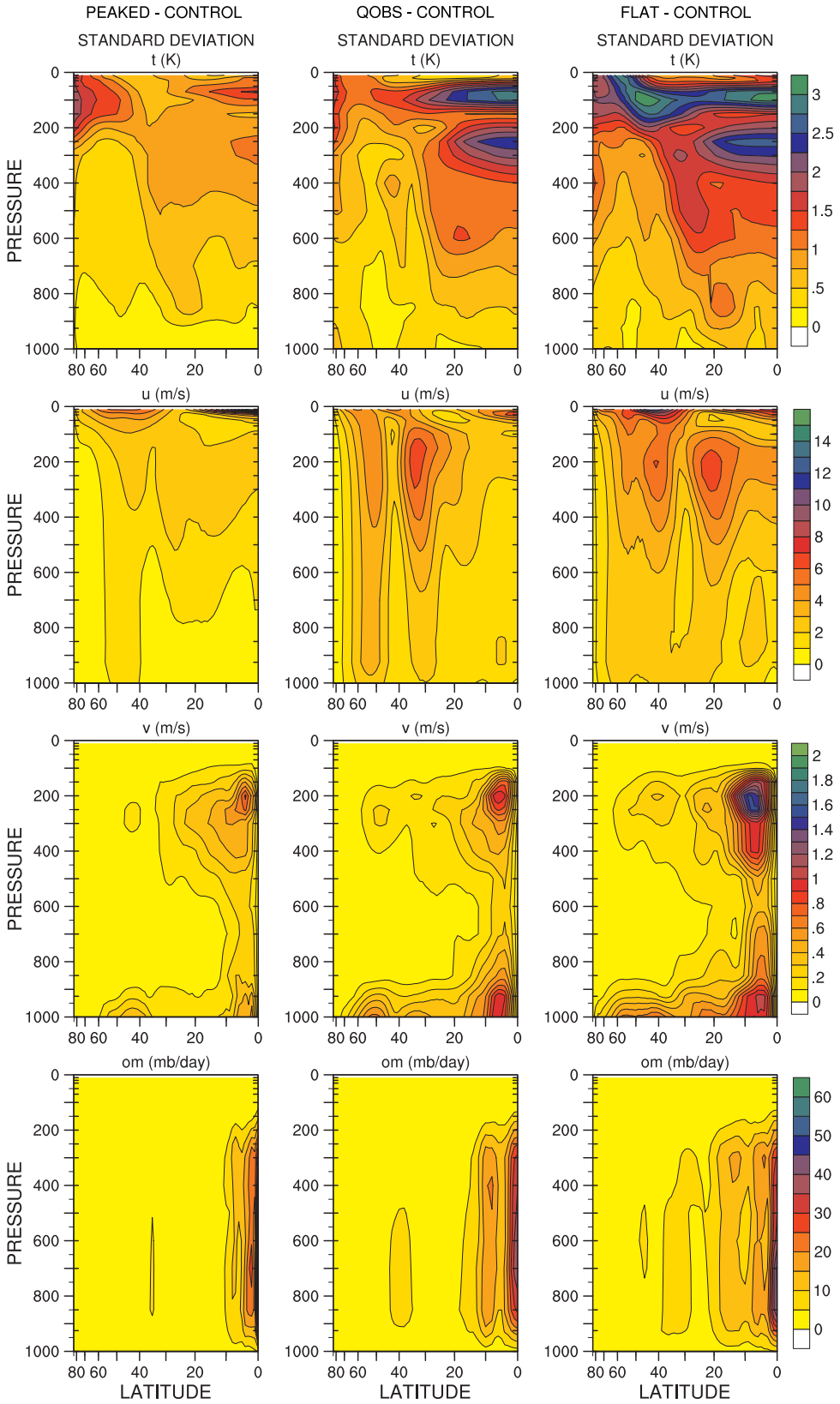

Figure 7: Inter-model standard deviation of the differences, experiment - control, of the zonal-time average for temperature (t), zonal wind (u), meridional wind (v), pressure vertical velocity (om) and relative humidity (rh) for PEAKED−CONTROL, QOBS−CONTROL and FLAT−CONTROL.

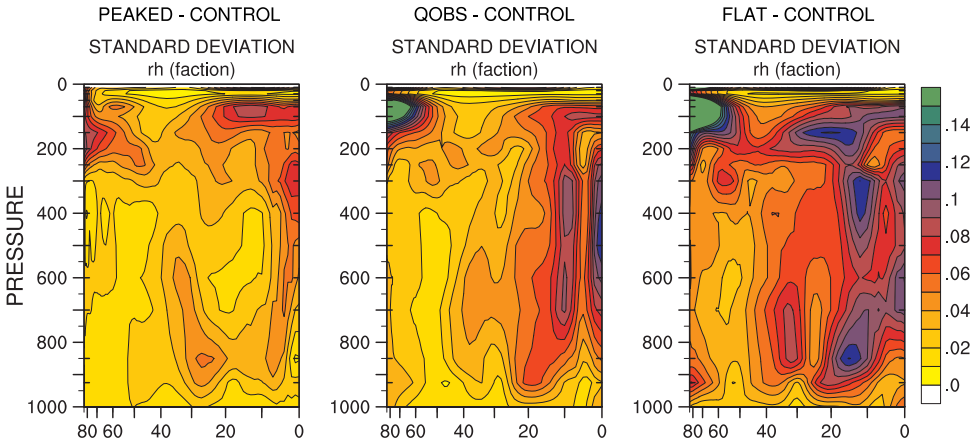

Figure 7 (continued): Inter-model standard deviation of the differences, experiment - control, of the zonal-time average for temperature (t), zonal wind (u), meridional wind (v), pressure vertical velocity (om) and relative humidity (rh) for PEAKED - CONTROL, QOBS - CONTROL and FLAT - CONTROL.

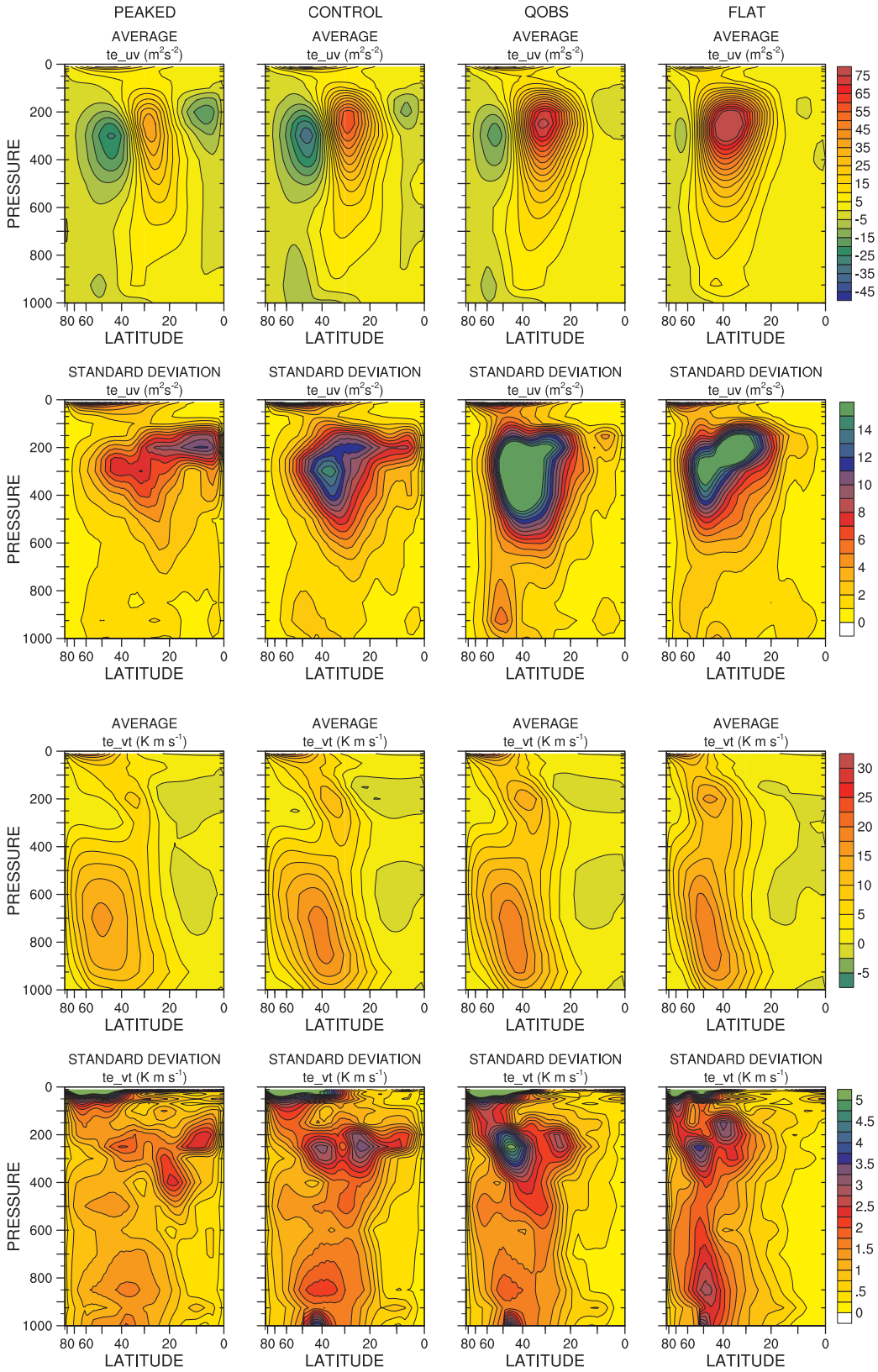

Figure 8: Multi-model mean and standard deviation, transient eddy momentum $\overline{[u'^* v'^*]}$ and heat fluxes $\overline{[v'^* T'^*]}$ for PEAKED, CONTROL, QOBS and FLAT.

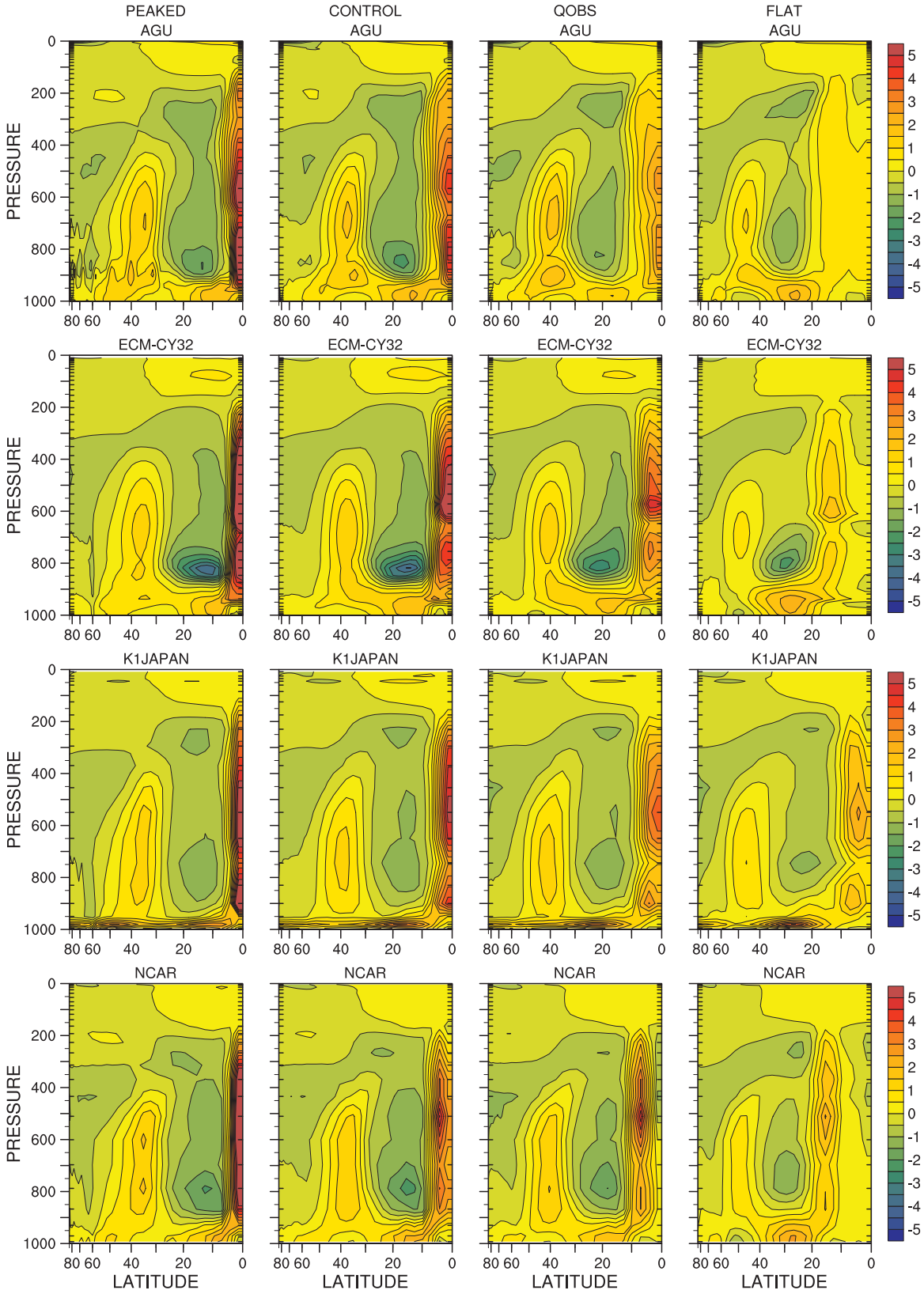

Figure 9: Parameterized total temperature tendency for individual models for PEAKED, CONTROL, QOBS and FLAT, K day^{-1}.

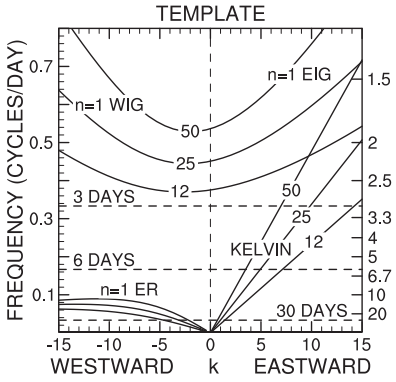

Figure 10: Template of dispersion curves for wavenumber-frequency diagrams of symmetric equatorial modes shown in Fig. 11.

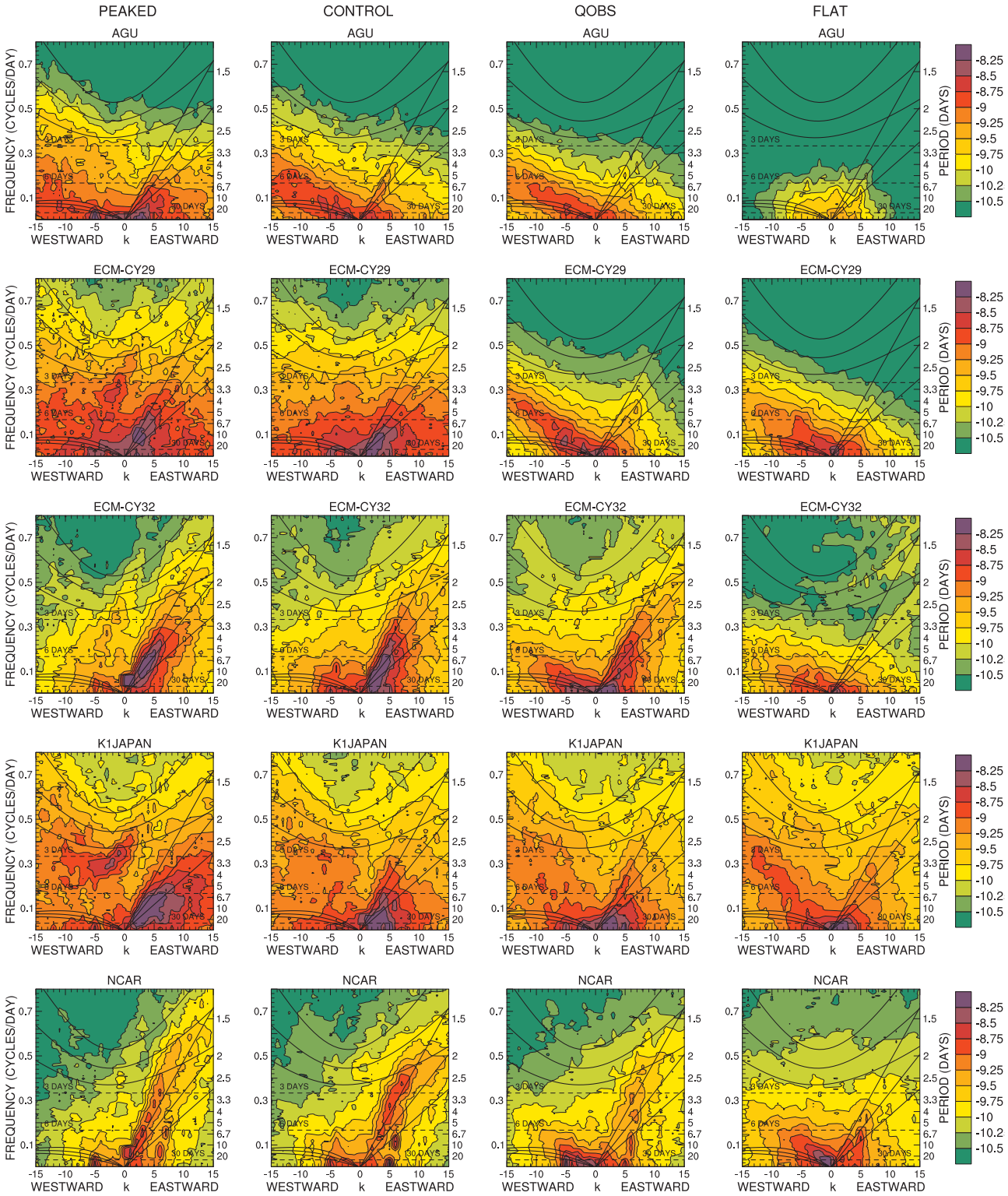

Figure 11: Wavenumber-frequency diagrams of log of power of symmetric modes of equatorial precipitation from AGU, ECM-CY29, ECM-CY32, K1JAPAN and NCAR for PEAKED, CONTROL, QOBS and FLAT, $-20°$ to $+20°$ latitude. The template for the dispersion curves is shown in Fig. 10.

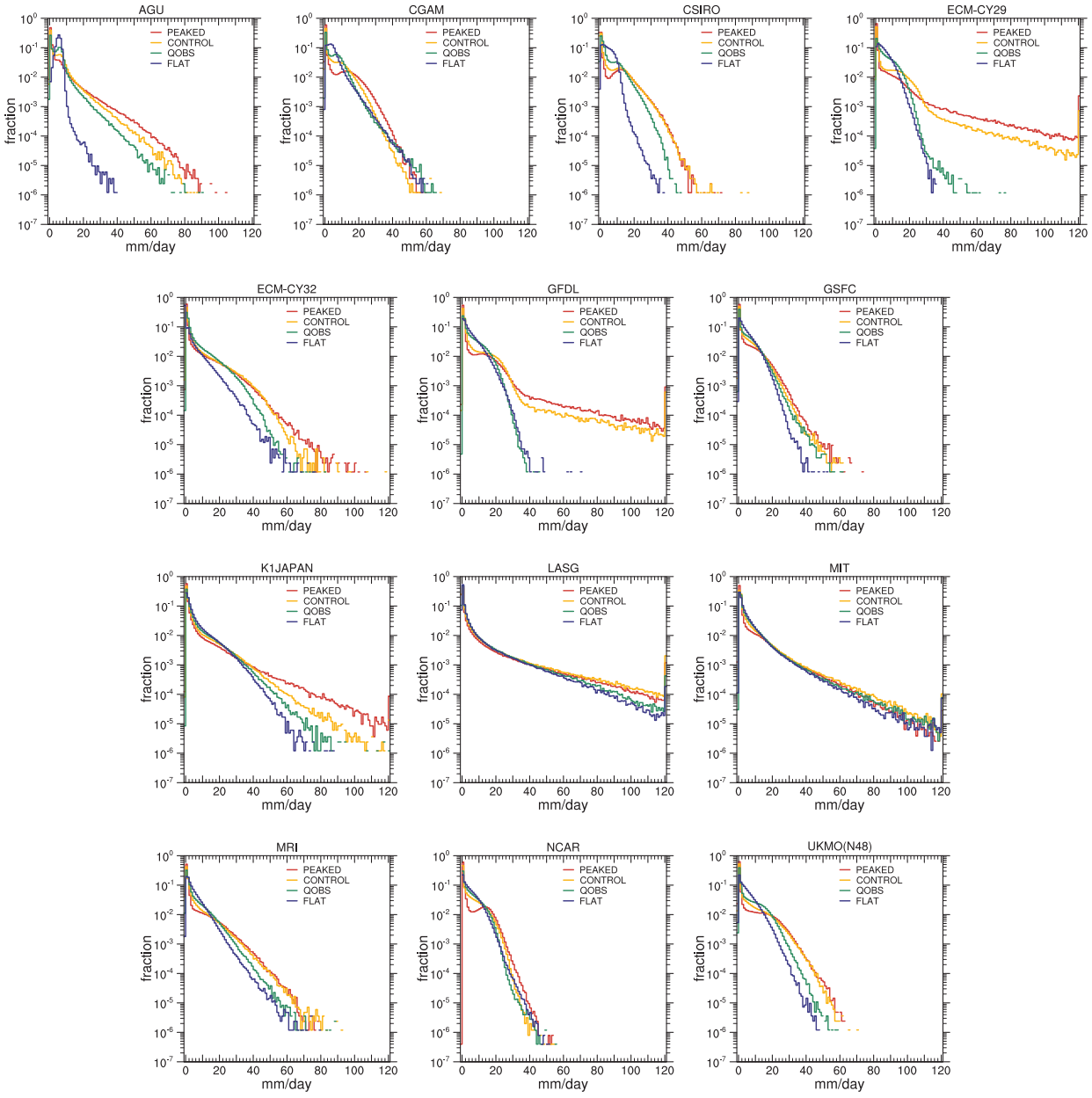

Figure 12: Fraction of time that 6 hour averaged precipitation from $-20°$ to $+20°$ latitude is in 1 mm day^{-1} bins ranging from 0 to 120 mm day^{-1} for individual models for PEAKED, CONTROL, QOBS and FLAT experiments. Grid values have been conservatively averaged to a 5° latitude-longitude grid.

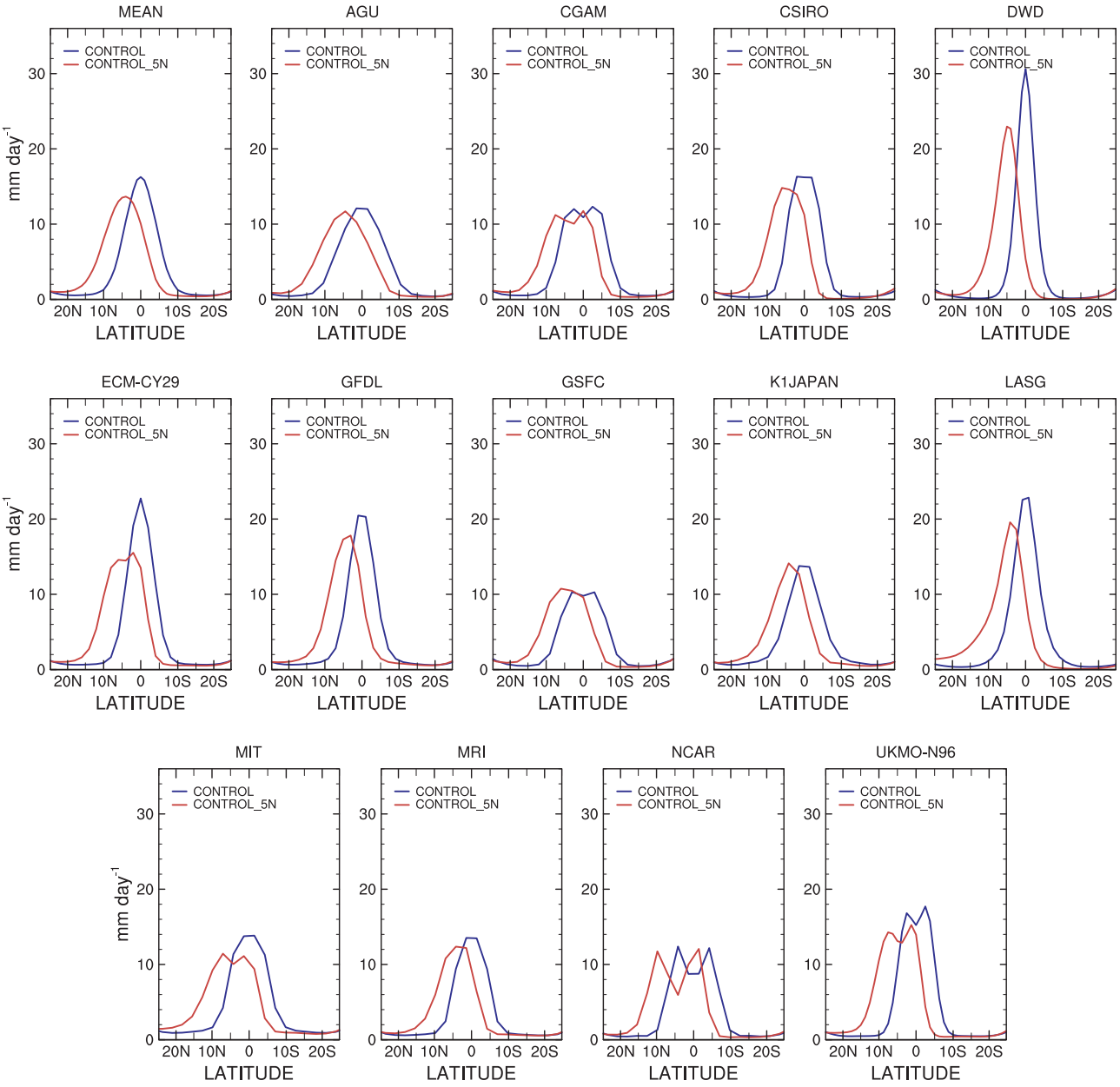

Figure 13: Zonal-time average precipitation for individual models from CONTROL and CONTROL_5N SST distributions, mm day^{-1}.

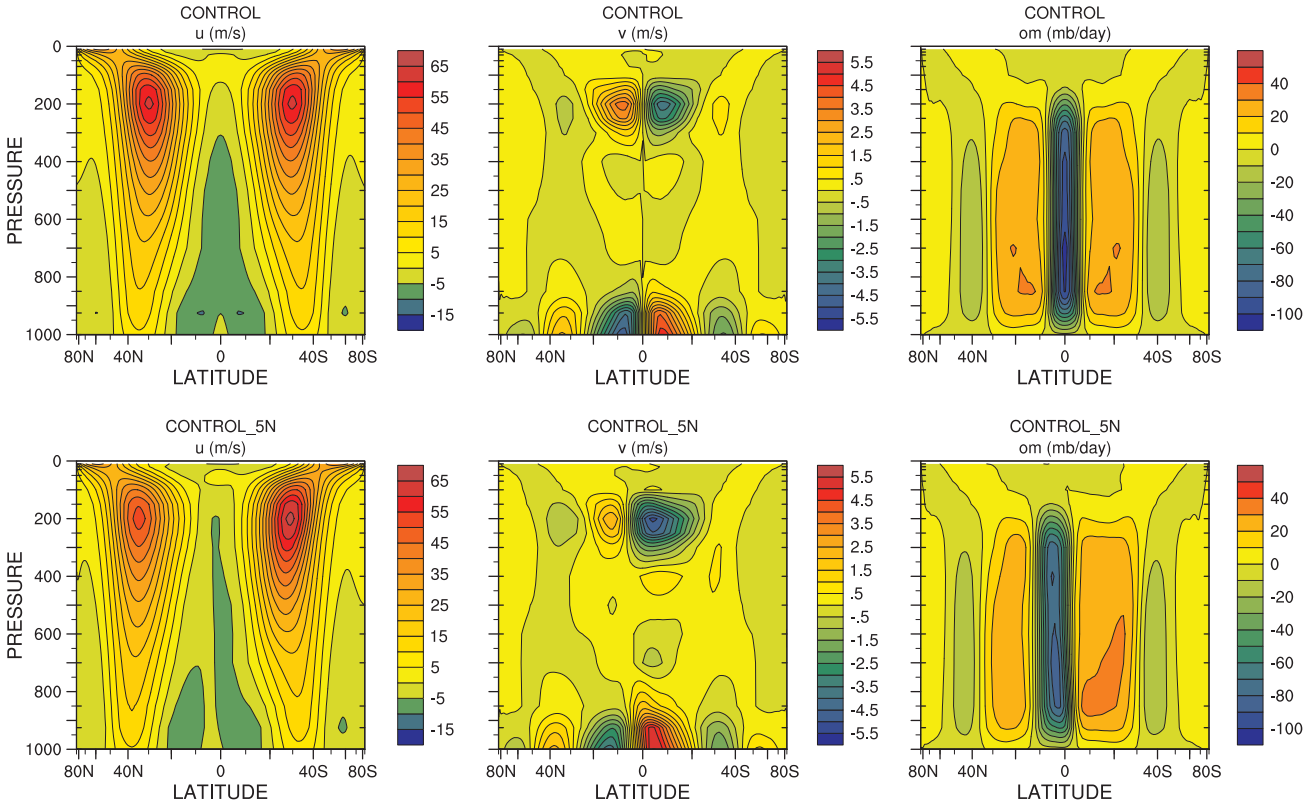

Figure 14: Zonal-time average multi-model mean u, v and omega for CONTROL (top) and CONTROL_5N (bottom).